

---

Electronic Theses and Dissertations, 2004-2019

---

2007

## Anchoring Energy And Pretilt Angle Effects On Liquid Crystal Response Time

Xiangyi Nie  
*University of Central Florida*



Part of the [Electrical and Electronics Commons](#)

Find similar works at: <https://stars.library.ucf.edu/etd>

University of Central Florida Libraries <http://library.ucf.edu>

This Doctoral Dissertation (Open Access) is brought to you for free and open access by STARS. It has been accepted for inclusion in Electronic Theses and Dissertations, 2004-2019 by an authorized administrator of STARS. For more information, please contact [STARS@ucf.edu](mailto:STARS@ucf.edu).

---

### STARS Citation

Nie, Xiangyi, "Anchoring Energy And Pretilt Angle Effects On Liquid Crystal Response Time" (2007).  
*Electronic Theses and Dissertations, 2004-2019*. 3281.

<https://stars.library.ucf.edu/etd/3281>

# **ANCHORING ENERGY AND PRETILT ANGLE EFFECTS ON LIQUID CRYSTAL RESPONSE TIME**

by

**XIANGYI NIE**

B.S. Nanjing University, P.R. China, 1999

M.S. Nanjing University, P.R. China, 2002

M.S. University of Central Florida, USA, 2004

A dissertation submitted in partial fulfillment of the requirements  
for the degree of Doctor of Philosophy  
in the School of Electrical Engineering and Computer Science  
in the College of Engineering and Computer Science  
at the University of Central Florida  
Orlando, Florida

Fall Term  
2007

Major Professors: Shin-Tson Wu  
Thomas X. Wu

## ABSTRACT

This dissertation covers some important topics on the liquid crystal-substrate surface effects, including theoretical derivations and confirming experimental results. The research work is expected to make important impacts on liquid crystal device designs and to open new doors for further research along these topics.

In this dissertation, a novel high-electric-field technique is developed to characterize the anchoring energy of vertically-aligned liquid crystal cells. Both theoretical analyses and confirming experimental results are presented. Vertically-aligned liquid crystal cells with buffed polyimide alignment layers are used to validate the measurement techniques. Based on the voltage-dependent transmittance of the liquid crystal cells, a linear fitting can be obtained, which leads to a precise determination of the anchoring energy. If some specific liquid crystal material parameters are known, then the traditional cell capacitance measurements can be avoided.

Anchoring energy and cell gap effects on liquid crystal response time is theoretically analyzed and experimentally investigated. A novel theory on the liquid crystal dynamics is developed. In this part, two different theoretical approaches are discussed: one is *surface dynamic equation method* and the other is *effective cell gap method*. These two different approaches lead to consistent results, which are also confirmed by our experimental results. This work opens a new door for LCD industry to optimize liquid crystal response time, and it is especially critical for liquid crystal cells with thin cell gap, which is a promising approach for fast response time liquid crystal display.

Pretilt angle effects on liquid crystal dynamics are analyzed theoretically and validated experimentally. Analytical expressions are derived to describe liquid crystal response time under nonzero pretilt angle conditions. The theoretical analysis is confirmed experimentally

using vertically-aligned liquid crystal cells. These results quantitatively correlate pretilt angles with liquid crystal response time, which is important for optimizing liquid crystal response time.

To my parents, wife, and daughter

## ACKNOWLEDGMENTS

I would like to thank those who contributed and supported my efforts throughout my graduate studies at the University of Central Florida.

First of all, I would like to sincerely thank my advisor, Dr. Shin-Tson Wu, for his constant and precious help, motivation, and guidance. Without his valuable advises and instructions, it is impossible for me to accomplish these research works. I also would like to thank him for his kind instructions and patience to improve my oral English in presentations and written English in publications.

I am truly indebted to my advisor, Dr. Thomas X. Wu for his enlightening discussion and advice. I would like to thank him for his patience and time to teach me the numerical simulation techniques and electromagnetics, which are critical throughout my research work. His kind help for my life in the United States is also truly appreciated.

I would also like to thank my dissertation committee members, Dr. Jiann S. Yuan, Dr. Parveen F. Wahid, and Dr. John Shen, for their help and valuable suggestions about my dissertation.

I gratefully acknowledge all the postdoctoral fellows in the Photonics and Display group for their stimulating discussions and technical assistance, particularly Dr. Yanqing Lu, Dr. Xinyu Zhu, Dr. Ruibo Lu, and Dr. Haiqing Xianyu.

I am grateful to all the students in the Photonics and Display group and High-Speed Electronic System group; I would like to thank them for their help and encouragement.

Finally, I would like to give special thanks to my wife, Ying Lou. She gave up her career in China and came to the United States with me. She has always been supporting me wholeheartedly. I am also very appreciated to my parents for their full support. Without my

wife and parents' support and sacrifice, the accomplishment of my education is impossible.

# TABLE OF CONTENTS

LIST OF FIGURES .....	x
LIST OF TABLES.....	xiv
LIST OF ACRONYMS/ABBREVIATIONS .....	xv
CHAPTER ONE: INTRODUCTION.....	1
1.1 Motivation.....	1
1.2 Liquid Crystal Materials .....	2
1.3 Basic Physical Properties of Liquid Crystals.....	4
1.3.1 Birefringence.....	5
1.3.2 Dielectric Anisotropy.....	5
1.3.3 Visco-elastic Properties .....	8
1.3.3.1 Elastic Constants.....	8
1.3.3.2 Rotational Viscosity.....	10
1.3.3.3 Figure of Merit.....	10
1.4 Introduction to Liquid Crystal Alignment .....	12
1.4.1 Rubbing method.....	12
1.4.2 Photoalignment .....	13
1.4.3 Pretilt Angle.....	14
1.5 Anchoring Energy.....	15
1.6 Thesis Overview .....	18
CHAPTER TWO: NUMERICAL SIMULATION METHODOLOGIES .....	19
2.1 Simulation of LC Director Distribution.....	19
2.1.1 Static State Simulation.....	20
2.1.2 Dynamic Process Simulation .....	21

2.2 Optical Simulation .....	23
2.3 Static Simulation of Anchoring Energy Effects on Electro-optic Response of LC Cells...	24
2.4 Dynamic Simulation of Dual-Frequency Liquid Crystal Device .....	26
2.5 Simulation of Phase Retardation Dependent Liquid Crystal Electro-optic Modulation.....	29
CHAPTER THREE: POLAR ANCHORING ENERGY MEASUREMENT .....	39
3.1 Introduction.....	39
3.2 Theory of Anchoring Energy Measurement by Fredericksz Transition .....	41
3.3 Theory of Anchoring Energy Measurement by High-Electric-Field Method .....	42
3.4 Experiment.....	48
3.5 Discussion .....	54
CHAPTER FOUR: ANCHORING ENERGY AND CELL GAP EFFCTS ON LIQUID CRYSTAL RESPONSE TIME.....	56
4.1 Introduction.....	56
4.2. Theory .....	57
4.2.1 Effective Cell Gap Method .....	57
4.2.2 Surface Dynamic Equation Method.....	62
4.2.3 Results and Discussion .....	64
4.3 Experiment.....	68
4.4 Discussion of Thin Cell Gap Effect.....	71
4.5 Summary .....	74
CHAPTER FIVE: PRETILT ANGLE EFFECTS ON LIQUID CRYSTAL RESPONSE TIME.....	76
5.1 Introduction.....	76
5.2 Theory .....	76
5.3 Experiment.....	81

CHAPTER SIX: CONCLUSION .....	88
LIST OF REFERENCES .....	90

## LIST OF FIGURES

Figure 1.1: Schematics of three thermotropic LCs: (a) nematic, (b) smectic, and (c) cholesteric .....	3
Figure 1.2: Illustration of birefringence .....	5
Figure 1.3: Illustration of LC dielectric anisotropy .....	6
Figure 1.4: Frequency dependent dielectric anisotropy $\Delta\epsilon$ of a dual-frequency liquid crystal. When the frequency of the driving voltage is lower than the crossover frequency $f_c$ , $\Delta\epsilon > 0$ , and when it is higher than $f_c$ , $\Delta\epsilon < 0$ . Through frequency modulation, fast rise and decay times can be obtained. ....	8
Figure 1.5: Demonstrations of three basic deformations of an LC.....	9
Figure 1.6: Rubbing method .....	12
Figure 1.7: Photoalignment method.....	13
Figure 1.8: Pretilt angle prevents reverse tilt disclination of liquid crystal directors in electric field. ....	14
Figure 2.1: Anchoring energy $W$ dependent electro-optic responses of a $7 \mu\text{m}$ VA LC cell.....	25
Figure 2.2: Upper part of each figure shows the experiment result and simulation result, the under part shows the voltage and frequency modulation. Numerical simulation includes the dual frequency, overdriving and bias voltage effects, and it agrees well with the experimental results. ....	28
Figure 2.3: Voltage-dependent normalized transmittance of a homogeneous LC cell. Regions 2, 4, and 6 correspond to $\delta_0 \sim N\pi$ , and regions 1, 3, and 5 correspond to $\delta_0 \sim (N - \frac{1}{2})\pi$ .....	31

Figure 2.4: Experimental demonstration of $f_o=4f_e$ at $f_e=60\text{Hz}$ . The applied voltage $V_{pp}=14.87$ V and $\delta_0$ is around $1\pi$ .	33
Figure 2.5: Simulation results of $f_o=2f_p=4f_e$ , where $f_e=60\text{Hz}$ . In the simulation, $V_{pp}=13.8$ V is used to keep $\delta_0\sim\pi$ , and peak-to-peak phase shift $\Delta\delta\sim0.19\pi$ . Then $f_o=4f_e$ because the $\Delta\delta$ exists at the maximum point of optical transmittance, that is, around region 2 in Figure 2.3.	34
Figure 2.6: Experimental demonstration of $f_o=2f_e$ and $f_e=60\text{Hz}$ . The peak-to-peak driving voltage $V_{pp}=11.81$ V and $\delta_0\sim1.5\pi$ .	35
Figure 2.7: Simulation results of $f_o=2f_e$ , and $f_e=60$ Hz. In the simulation, $V_{pp}=11.80$ V is used to keep $\delta_0\sim1.5\pi$ , which is around region 2 of Figure 2.3. The $\Delta\delta$ peak-to-peak amplitude is $0.17\pi$ .	36
Figure 3.1: Schematic drawing of the LC director distribution of a VA cell. Left: $V=0$ and right: $V\gg V_{th}$ . The LC directors near the substrate surfaces could be reoriented when $V\gg V_{th}$ , and the reorientation depends on the anchoring energy $W$ .	42
Figure 3.2: Numerical simulation for the voltage dependent $\Delta\phi_{max}$ , which validates the assumption of $\Delta\phi_{max}\approx\pi/2$ when $V>4V_{th}$ . The LC mixture used for simulation is Merck MLC-6608: $K_{11}=16.7$ pN, $K_{33}=18.1$ pN, $\varepsilon_{  }=3.6$ , $\varepsilon_{\perp}=7.8$ , $\gamma_1=0.186$ Pas, $n_o=1.475$ , and $n_e=1.558$ .	44
Figure 3.3: Experimental setup for measuring the anchoring energy of VA cells. A VA cell is placed between crossed polarizer and analyzer. The optical axis of the VA cell is oriented at $45^\circ$ with respect to the polarizer.	48
Figure 3.4: Voltage-dependent $CV$ curve of a $7\ \mu\text{m}$ VA cell filled with MLC-6608. In the high voltage region, a linear curve is observed and the intercept at $CV=0$ is $1.24 V_{rms}$ .	50

Figure 3.5: Illustration of the intercept extrapolation method described in Eq.(3.6). A linear fitting is obtained in the  $V > 8 V_{\text{rms}}$  region. The intercept at  $1/CV=0$  leads to  $W=(3.0\pm 0.2)\times 10^{-4} \text{ J/m}^2$ . A  $7 \mu\text{m}$  VA cell filled with MLC-6608 is used as an example..... 51

Figure 3.6: Illustration of the slope fitting method according to Eq.(3.7). A linear fitting between  $V=9 V_{\text{rms}}$  and  $18 V_{\text{rms}}$  is observed, and the anchoring energy is deduced as  $W=(3.1\pm 0.2)\times 10^{-4} \text{ J/m}^2$ . A  $7 \mu\text{m}$  VA cell filled with MLC-6608 is tested as an example.... 52

Figure 3.7: Illustration of the slope fitting method according to Eq.(3.10). A Linear fitting and a measurement result of  $W=(3.2\pm 0.3)\times 10^{-4} \text{ J/m}^2$  are obtained for the  $7 \mu\text{m}$  MLC-6608 VA cell. The LC cell capacitance measurement is avoided by adopting Eq.(3.8). ..... 53

Figure 4.1: Schematic drawing of a VA LC cell. .... 57

Figure 4.2: The z-coordinate dependent tilt angle  $\theta$ . The LC cell's physical surfaces are at  $z = \pm \frac{d}{2}$ . The  $\theta$  profile is extrapolated to  $z = \pm(\frac{d}{2} + b)$ , where  $\theta=0$ .  $b=K/W$  is the extrapolation length. .... 60

Figure 4.3: Anchoring energy ( $W$ ) and cell gap ( $d$ ) dependent LC decay time ( $\tau'_d = \tau'_o$ ). The solid lines represent the results of the effective cell gap method, and the dashed lines are based on the surface dynamic equation method. When  $W$  is large, the results of these two methods are almost identical as the bottom three curves ( $W=1\times 10^{-3}$ ,  $1\times 10^{-4}$  and  $5\times 10^{-5} \text{ J/m}^2$ ) show. .... 65

Figure 4.4: (a) When  $d \gg b$ , the extrapolation length approximation is accurate; (b) When  $d \sim b$ , the approximation is less accurate. .... 67

Figure 4.5: Experimental results of the cell gap dependent LC optical decay time. Stars are the measurement data. The solid line is the fitting curve using the effective cell gap method Eq. (4.9), and the pink dashed line is based on the surface dynamic equation

method. From fittings, the anchoring energy is found to be $W=5.6\times 10^{-5}$ J/m <sup>2</sup> . The red dotted lines represent the fitting curve using $\tau_o\sim d^{1.7}$ .	69
Figure 4.6: Numerical simulation results of cell gap and anchoring energy dependent LC response time(100%-10%). The cell gap d is between 0 ~6.0 $\mu$ m, and the anchoring energy $W=1\times 10^{-4}$ J/m <sup>2</sup> and $\sim\infty$ .	72
Figure 4.7: Numerical simulation results of thin cell gap(0.4~1 $\mu$ m) and anchoring energy dependent LC response time(100%-10%). Two anchoring energy cases are simulated: $W=1\times 10^{-4}$ J/m <sup>2</sup> and $W\sim\infty$ .	74
Figure 5.1: Voltage dependent $\theta_m$ . The LC parameters used for simulations are: $\Delta\varepsilon=-4.2$ , $V_{th}=2.19$ V <sub>rms</sub> , $K_{11}=16.7$ pN, and $K_{33}=18.1$ pN.	80
Figure 5.2: Voltage dependent transmittance curves of a 6.97 $\mu$ m VA cell at $\lambda=633$ nm. The solid line is the experimental result, and dotted and dashed lines represent the simulation results for $\theta_p=0.1^\circ$ and $10.5^\circ$ , respectively.	82
Figure 5.3: Time-dependent $\ln[\delta_0/\delta(t)]$ of the 6.97 $\mu$ m VA cell. Dots are experimental data and solid line is the fitting curve. The slope of the straight line is 0.0338/ms, and $\tau_o$ is found to be $\sim 59$ ms.	84
Figure 5.4: Pretilt angle $\theta_p$ dependent LC response time $\tau_o$ . Solid line represents the numerical solution of Erickson-Leslie equation [Eq.(5.1)]. The circle is the experimental result using LC mixture B. Dashed lines are the calculated results using Eq.(5.13), ( $K=K_{33}$ ), which employs the small angle and one-elastic constant approximations. Dotted lines are also calculated from Eq.(5.13), except that $K_{33}$ is replaced by $K=(K_{11}+K_{33})/2$ . Cell gap d =7.10 $\mu$ m, and bias voltage $V_b=3.63$ V <sub>rms</sub> .	86

## LIST OF TABLES

Table 4.1: Anchoring energy $W$ dependent $x$ value, where $x$ is the exponent of $\tau_o \sim d^x$ . The data are obtained from the fitting of solid lines in Figure 4.3.....	66
--	----

## LIST OF ACRONYMS/ABBREVIATIONS

LC	Liquid Crystal
LCD	Liquid Crystal Display
SLM	Spatial Light Modulator
TN	Twist Nematic
VA	Vertical-Aligned
IPS	In-Plane-Switching
OCB	Optically-Compensated-Bend
DFLC	Dual-frequency Liquid Crystal
FLC	Ferroelectric Liquid Crystal
PWM	Pulse-Width Modulation
FoM	Figure of Merit
PI	Polyimide
TFT	Thin Film Transistor
FEM	Finite element method
FDTD	Finite-Difference Time-Domain
LCOS	Liquid-Crystal-On-Silicon
PVA	Patterned Vertical Alignment
MVA	Multi-domain Vertical Alignment
RGB	Red, green and blue

# CHAPTER ONE: INTRODUCTION

## 1.1 Motivation

Liquid crystal (LC) is a multi-disciplinary subject, which is related to optics, materials science, and electronics. It has been widely used in both display and photonics fields. Nowadays, liquid crystal displays (LCDs) can be found everywhere, for examples, in handheld devices (such as PDAs, cell phones and music players), notebook computers, desktop monitors, LCD TVs, and car navigations. In photonics area, various liquid crystal spatial light modulators (SLMs) have been used for laser beam steering, tunable-focus lens, and other photonic devices. Active research work has been focused on the liquid crystal technology, and it is being improved remarkably in recent years.

An LC device usually includes at least one LC cell, where the liquid crystal material is sandwiched between two layers of substrates. Liquid crystal molecules would be randomly distributed in the cell if there is no alignment treatment on the substrates. Some special cases do exist, such as polymer-dispersed liquid crystal (PDLC) in which surface alignment is not needed. Most of LC devices do need surface treatment. In order to align liquid crystal molecules, surface-induced alignments are necessary. Various LCD modes have been developed, such as Twisted Nematic (TN), Vertical Alignment (VA), Homogeneous Alignment, In-Plane-Switching (IPS), and Optically-Compensated-Bend (OCB) modes. All these LCD modes rely on the surface alignment techniques, which align the LC molecules on the LC cell substrates.

Although the alignment techniques have been actively studied for years, the surface effects on the electro-optic and dynamic performances of LC devices have not been well understood yet. In this dissertation, we focus on the characterization of LC-substrate surface properties and the surface effects on LC device performance. The anchoring energy and pretilt angle effects on the LC response time are studied and results discussed.

## **1.2 Liquid Crystal Materials**

Liquid crystal material only occupies a small portion in an LC device, but it plays a key role in determining the device performance. An LC mode is jointly determined by the LC material employed and its molecular alignment. Therefore, they both play fundamental roles in an LC technology.

If liquid crystal is considered from the structural point of view, it is an intermediate state between the solid crystals and isotropic liquids [1]. Like ordinary isotropic liquids, liquid crystal has flow and conformability properties. But if it is in a cell and aligned by surface treatment, liquid crystal has similar properties as solid crystals, including optical, dielectric, and elastic anisotropies. There are three types of LCs: thermotropic, lyotropic, and polymeric. Among these three, thermotropic LCs have been extensively studied. As illustrated in Figure 1.1, thermotropic LCs can exist in three phases: nematic, smectic, and cholesteric.

Figure 1.1(a) shows the nematic phase. The rod-like nematic LC molecules are lined up to a preferred direction, which is characterized by a unit vector  $\mathbf{n}$  called LC director. When an external voltage is applied to the LC cell, and if it is over the Freedericksz transition

threshold, the LC director will be reoriented by the electric field. Liquid crystals are birefringent materials, and the reorientation of LC directors will induce phase retardation or phase change on the incoming electromagnetic waves. In an LCD, the visible light is modulated by the voltage-induced LC reorientation. The nematic LCs have relatively simple molecular alignment. They can also generate natural gray scales easily. Therefore, nematic LCs have become the mainstream for display and tunable photonics applications. In this dissertation, our discussion is focused on the nematic phase.

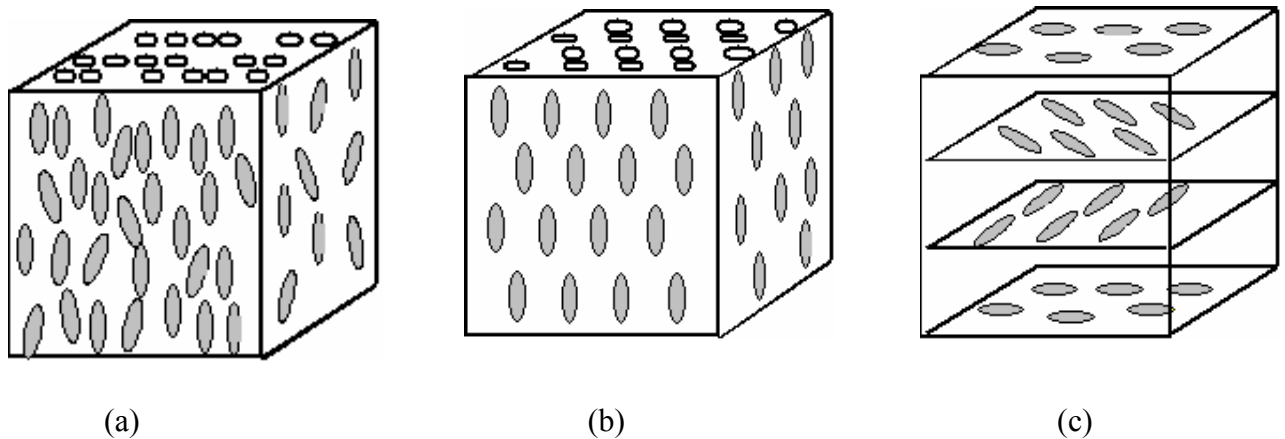


Figure 1.1: Schematics of three thermotropic LCs: (a) nematic, (b) smectic, and (c) cholesteric.

In the smectic phase shown in Figure 1.1(b), the molecules are in layered structures and arrange well with each other. An exciting feature of the chiral smectic-C phase is that it exhibits ferroelectricity. Using its spontaneous polarization, the response time of a bistable ferroelectric liquid crystal (FLC) modulator is in the 10-100  $\mu\text{s}$  range. FLC has been

demonstrated on a silicon backplane for virtual and projection displays [2]. Due to its fast response time, the FLC can use pulse-width modulation (PWM) approach to obtain gray scales.

In the cholesteric phase shown in Figure 1.1(c), it is thermodynamically equivalent to nematic phase except for the chiral-induced helix in the directors. There is parallel ordering in the same plane, but helical rotation along the axis perpendicular to different planes. The LC directors follow the helical rotation of the chiral agents. The polarization states of the reflected and transmitted waves depend on the pitch length of the cholesteric. The bistability nature leads to low power consumption, thus, cholesteric display is an attractive candidate for electronic books [3].

### **1.3 Basic Physical Properties of Liquid Crystals**

The molecular arrangement of nematic liquid crystal exhibits a certain degree of order. It results in anisotropy of the mechanical, electrical, magnetic, and optical properties. These unique characteristics make LC particularly suitable for electro-optic applications. For a nematic LC device, birefringence, elastic constants, dielectric anisotropy, and rotational viscosity all significantly influence the device performance. In the following sections, a brief introduction is given on basic physical properties of LC materials.

### 1.3.1 Birefringence

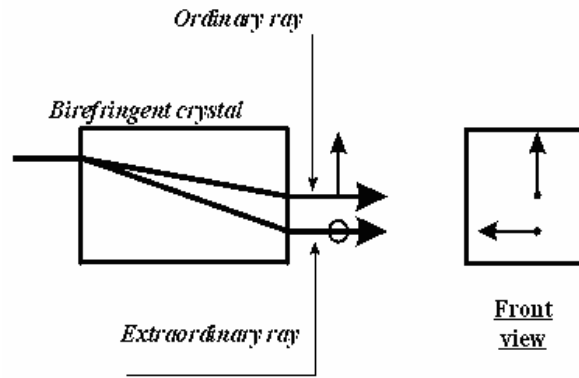


Figure 1.2: Illustration of birefringence

As shown in Figure 1.2, a uniaxial liquid crystal exhibits different refractive indices for the extraordinary ray ( $n_e$ ) and the ordinary ray ( $n_o$ ), and the difference is called as birefringence ( $\Delta n = n_e - n_o$ ). For both display and optical communication applications, high birefringence LC materials are important [4]. The birefringence effect on LC response time is through the cell gap dependence. A high birefringence LC material leads to a thinner cell gap which, in turn, reduces the response time. In order to describe the refractive index dispersion of LC materials, wavelength and temperature effects need to be taken into account. The details are discussed in Refs. [5,6,7].

### 1.3.2 Dielectric Anisotropy

The static dielectric permittivity  $\epsilon$  of an isotropic non-associated liquid can be approximately expressed by Onsager equation [8]. The dielectric anisotropy is defined

as  $\Delta\varepsilon = \varepsilon_{\parallel} - \varepsilon_{\perp}$ , where  $\varepsilon_{\parallel}$  and  $\varepsilon_{\perp}$  are the dielectric permittivities parallel and perpendicular to the director, respectively. The LC materials with a large dielectric anisotropy are desired for low operating voltage. Low operating voltage will result in low power consumption, which is very critical for mobile displays.

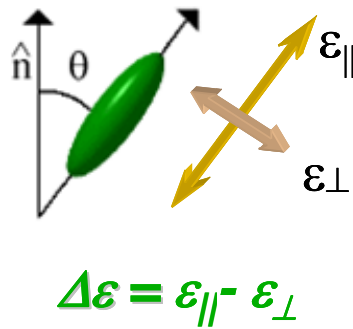


Figure 1.3: Illustration of LC dielectric anisotropy

From the molecular point of view, the dielectric anisotropy originates from the anisotropic distribution of the molecular dipoles in the liquid crystal phases. Nematic phases formed by elongated molecules carrying longitudinal and transverse dipoles have positive and negative dielectric anisotropy, respectively. The magnitude of dielectric anisotropy increases with that of the molecular dipoles and with the degree of ordering.

In Maier and Meier's theory [9], the Onsager theory is extended to nematic LC. An LC molecule is represented by an anisotropic polarizability  $\alpha$  with principal elements  $\alpha_l$  and  $\alpha_t$  in spherical cavity of radius  $a$ . Denoting the dipole moment with  $\alpha_l$  at an angle  $\theta$ , the LC dielectric components  $\varepsilon_{\parallel}$ ,  $\varepsilon_{\perp}$  and  $\Delta\varepsilon$  can be expressed as

$$\varepsilon_{||} = NhF \left\{ \langle \alpha_{||} \rangle + (F\mu^2 / 3kT) [1 - (1 - 3 \cos^2 \theta)S] \right\}, \quad (1.1)$$

$$\varepsilon_{\perp} = NhF \left\{ \langle \alpha_{\perp} \rangle + (F\mu^2 / 3kT) [1 + (1 - 3 \cos^2 \theta)S / 2] \right\}, \quad (1.2)$$

$$\Delta\varepsilon = NhFS \left\{ (\alpha_{||} - \alpha_{\perp}) - (F\mu^2 / 2kT) (1 - 3 \cos^2 \theta) \right\}, \quad (1.3)$$

where  $N$  is the molecular packing density,  $\mu$  is the dipole moment,  $F$  is the Onsager reaction field and  $\langle n \rangle$  is average refractive index. Here  $h$  and  $F$  are dependent on the average dielectric constant  $\langle \varepsilon \rangle$  and average refractive index  $\langle n \rangle$ :

$$h = \frac{3\langle \varepsilon \rangle}{2\langle \varepsilon \rangle + 1}, \quad (1.4)$$

$$F = \frac{(2\langle \varepsilon \rangle + 1)(\langle n \rangle^2 + 2)}{3(2\langle \varepsilon \rangle + \langle n \rangle^2)}. \quad (1.5)$$

Based on Eq.(1.3), the dielectric anisotropy of an LC material is influenced by three factors: molecular structure, temperature, and frequency. Here we only discuss the frequency effect, since the simulation of DF-LC will be discussed in Chapter Two.

Frequency dependent dielectric constant is an important factor for DF-LC material. As shown in Figure 1.4, at low frequencies  $\Delta\varepsilon > 0$ , while at high frequencies  $\Delta\varepsilon$  could become negative. As  $f$  increases,  $\varepsilon_{||}$  decreases while  $\varepsilon_{\perp}$  stays constant, which results in a decreased  $\Delta\varepsilon$ . The dielectric anisotropy  $\Delta\varepsilon$  changes sign at the crossover frequency  $f_c$ . For a pure LC compound, its  $f_c$  is usually higher than 10 MHz, which is too high to be useful for practical applications. In a dual-frequency LC mixture, positive and negative  $\Delta\varepsilon$  LC compounds are mixed and  $f_c$  is usually lower than  $\sim 10$  kHz. Then dual-frequency effect can be a useful approach for achieving fast response time.

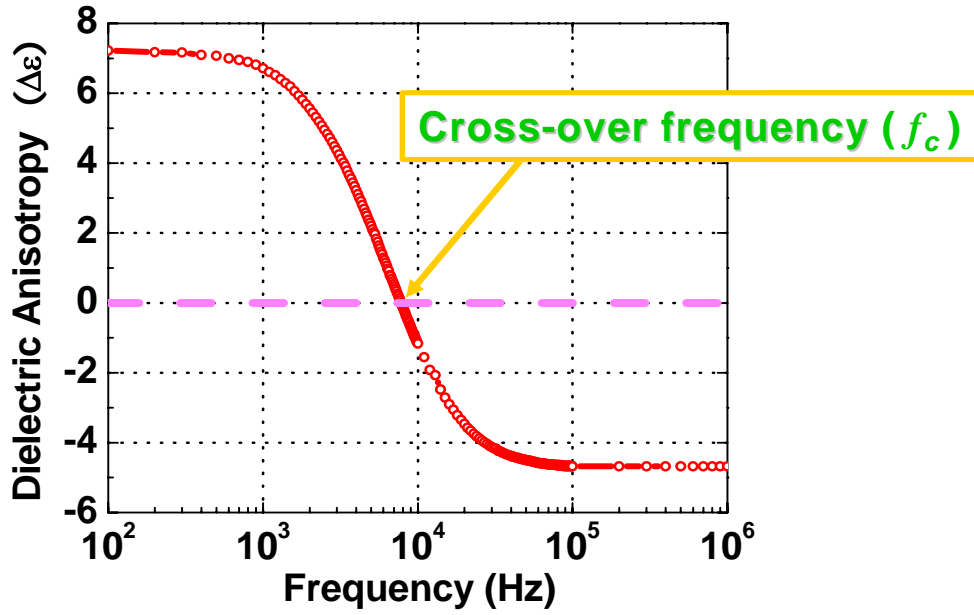


Figure 1.4: Frequency dependent dielectric anisotropy  $\Delta\epsilon$  of a dual-frequency liquid crystal. When the frequency of the driving voltage is lower than the crossover frequency  $f_c$ ,  $\Delta\epsilon > 0$ , and when it is higher than  $f_c$ ,  $\Delta\epsilon < 0$ . Through frequency modulation, fast rise and decay times can be obtained.

### 1.3.3 Visco-elastic Properties

Birefringence is not the only critical parameter for an LC material, instead, Figure of Merit which is defined as  $FoM = \frac{K_{11}\Delta n^2}{\gamma_1}$  represents the overall LC material performance. FoM includes not only the birefringence, but also the elastic constant and viscosity parameters of an LC material. In this part, both parameters will be introduced.

#### 1.3.3.1 Elastic Constants

The Frank energy (free volume elastic energy) density of nematic liquid crystal can be

written as:

$$f_{elastic} = \frac{1}{2}K_{11}(\nabla \cdot \vec{n})^2 + \frac{1}{2}K_{22}(\vec{n} \cdot \nabla \times \vec{n})^2 + \frac{1}{2}K_{33}(\vec{n} \cdot \nabla \cdot \vec{n})^2, \quad (1.6)$$

where  $K_{11}$ ,  $K_{22}$ , and  $K_{33}$  represent the elastic constants associated with splay, twist, and bend deformation, as shown in Figure 1.5.

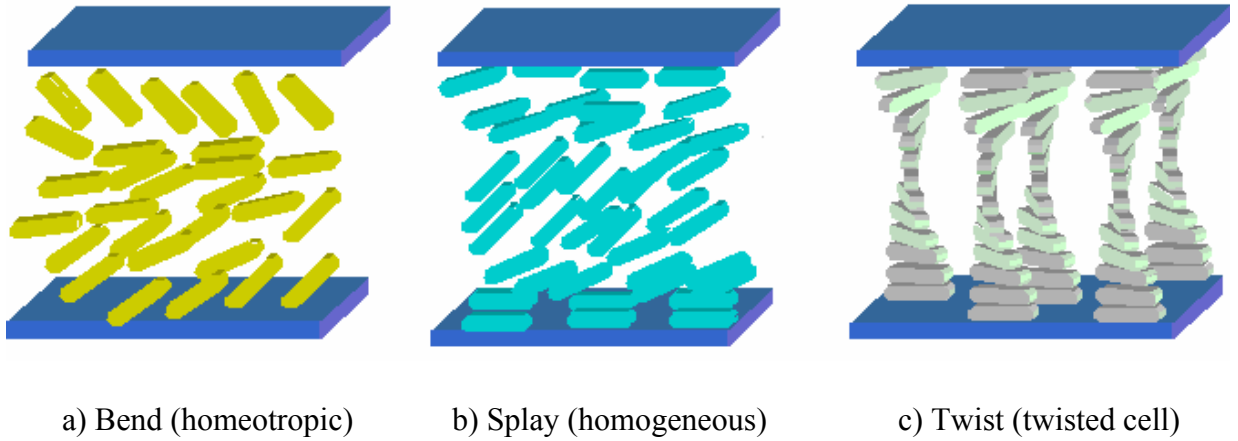


Figure 1.5: Demonstrations of three basic deformations of an LC.

Each of the elastic constants is related to an alignment mode of LC cells, in that  $K_{11}$  for homogeneous cell,  $K_{22}$  for twisted cell, and  $K_{33}$  for homeotropic cell. The elastic constants are linearly proportional to  $S^2$ , based on the Maier-Saupe theory:

$$K_{33} > K_{11} > K_{22} \sim S^2. \quad (1.7)$$

Here  $S$  is the order parameter and it describes the orientation order of a liquid crystal material. For a completely random and isotropic LC material,  $S=0$ , and for a perfectly aligned LC material,  $S=1$ . For a typical liquid crystal sample,  $S$  is on the order of 0.3 to 0.8, and generally decreases as the temperature is raised.

Elastic constants influence the operation voltage and response time of an LC device. A larger elastic constant not only leads to a higher operation voltage but also increases the response time, which is proportional to  $1/K_{ij}$ . Details will be discussed later.

### **1.3.3.2 Rotational Viscosity**

Response time is critical for almost all LC devices, and LC materials with low rotational viscosity  $\gamma_l$  are desired for fast response time. Both rise and decay times are linearly proportional to  $\gamma_l$ . The temperature-dependent rotational viscosity can be written as [10]:

$$\gamma_l = bS \exp(E / k_0 T), \quad (1.8)$$

where  $E$  is the activation energy,  $T$  is the Kelvin temperature, and  $k_0$  is the Boltzmann constant. From the molecular viewpoint, the rotational viscosity depends on the molecular constituents, dimensions, molecular interactions, and moment of inertia. A linearly conjugated liquid crystal should exhibit a relatively low rotational viscosity. At an elevated temperature,  $\gamma_l$  decreases dramatically. For every 10°C temperature increase, viscosity is roughly decreased by  $\sim 2X$ .

### **1.3.3.3 Figure of Merit**

Figure-of-Merit (FoM) takes both phase change and response time into consideration, and it is used to characterize the overall performance of an LC material. The FoM is defined as [4]:

$$FoM = \frac{K_{ii}\Delta n^2}{\gamma_1}, \quad (1.9)$$

where  $K_{ii}$  is the elastic constant, which may be  $K_{11}$ ,  $K_{22}$  or  $K_{33}$ , as mentioned previously,  $\Delta n$  is the birefringence, and  $\gamma_1$  is the rotational viscosity. All these parameters are temperature dependent. Both viscosity and elastic constants also depend on the order parameter  $S$  and can be approximated as:

$$\Delta n = (\Delta n)_0 S, \quad (1.10)$$

$$K_{ii} = aS^2. \quad (1.11)$$

The temperature dependent FoM is derived as:

$$FoM = (a/b)(\Delta n_0)^2 (1 - T/T_c)^{3\beta} \exp(-E/k_0T), \quad (1.12)$$

where  $\Delta n_0$  is the birefringence at  $S=1$ ,  $E$  is the activation energy of the liquid crystal and  $k_0$  is the Boltzmann constant. The value of the  $\beta$  parameter is around 0.20-0.25 and is not too sensitive to the liquid crystal structures.

## 1.4 Introduction to Liquid Crystal Alignment

### 1.4.1 Rubbing method

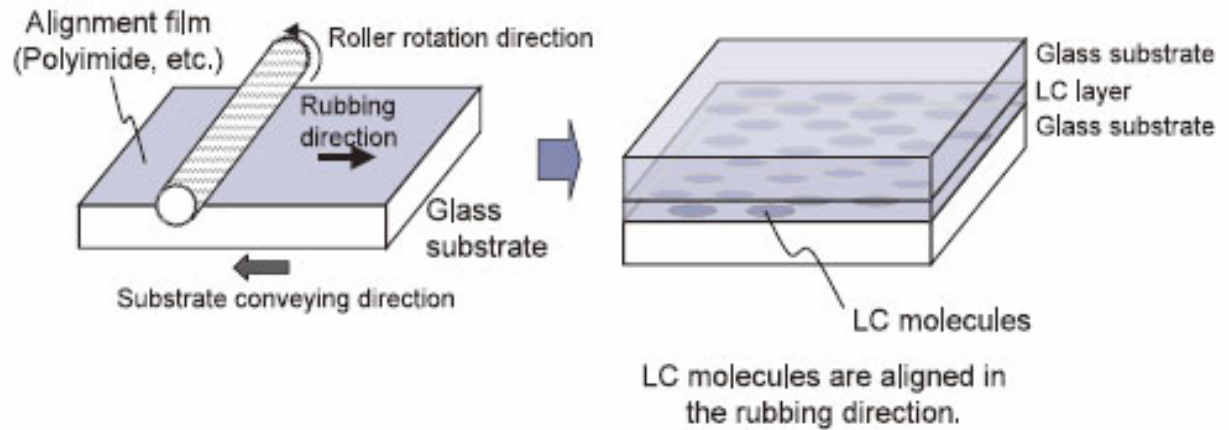


Figure 1.6: Rubbing method

As mentioned in the first chapter, surface alignment is critical for LC devices. Several surface alignment methods have been developed. The conventional and most widely used approach is the rubbing method, which is usually by moving a cloth over an LC cell substrate with thin organic film, such as polyimide (PI), polyvinyl alcohol, nylon, etc, as shown in Figure 1.6. A certain degree of polymer molecular orientation order which is called the pretilt angle is induced by the rubbing process. The orientation order is transmitted to the LC molecules anchored on the substrates, and is also further transmitted into the liquid crystal molecules in the bulk region via intermolecular forces [11]. The rubbing method is relatively simple, but it could cause contamination, static charges and mechanical damages. The

generated static charges could affect the performances of thin-film-transistors (TFTs) fabricated on the substrate. These problems could degrade the manufacturing yields of LCDs.

Therefore, some other alignment techniques like photoalignment, oblique angle SiO<sub>2</sub> evaporation, and ion beam etching are being actively studied.

### 1.4.2 Photoalignment

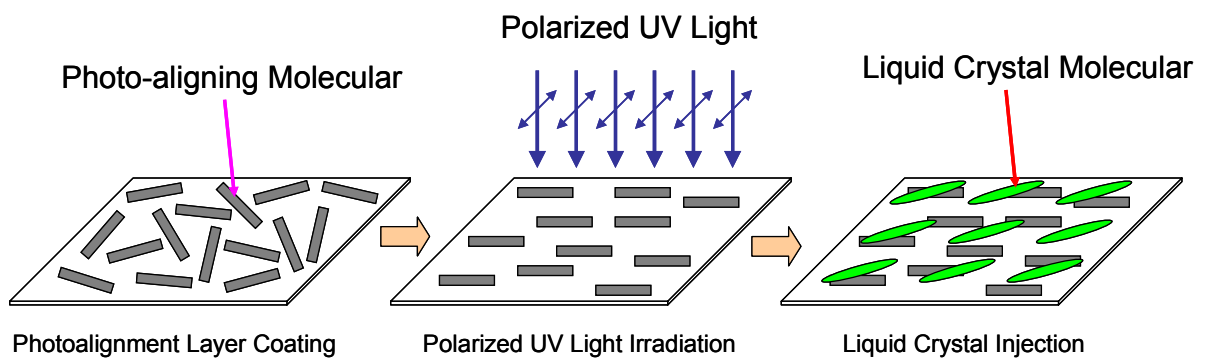


Figure 1.7: Photoalignment method

Photoalignment is a promising method for reducing the above mentioned disadvantages of mechanical rubbing. As shown in Figure 1.7, a layer of photo sensitive polymer is deposited on a substrate. Linearly polarized UV light induce certain degree of surface ordering on the layer, which further transfer the orientation order to the liquid crystal material. Usually, compared to rubbing method, photoalignment method generates weaker anchoring energy, which is the energy to fix liquid crystal molecules to their easy axis.

Photoalignment is a non-contact technique and it has a great advantage of imposing no mechanical and electrostatic damage to the alignment layer. The method also can be used to sequentially align liquid crystal material using different masks, which may induce complex alignment patterns [12,13].

Some other alignment techniques are also proposed, like amorphous carbon alignment layers and alignment by nanostructuring polymer surface. They all have their own advantages, but are not mainstream approaches currently.

### 1.4.3 Pretilt Angle

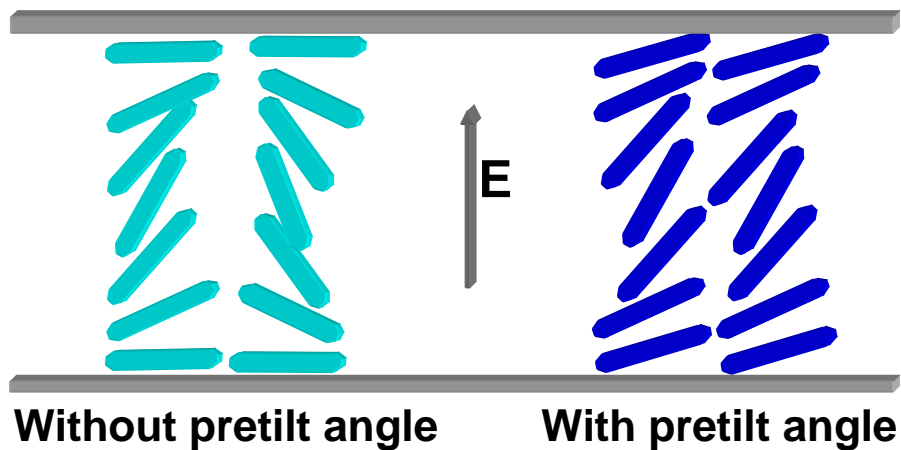


Figure 1.8: Pretilt angle prevents reverse tilt disclination of liquid crystal directors in electric field.

When external electric field is applied on LC cells, an appropriate pretilt angle of LC molecules on the LC-Substrate surfaces is necessary for most LCD devices. The pretilt angle

is to prevent LC molecules from reverse tilt disclinations. Both rubbing and photoalignment methods can induce pretilt angle. Recently, the control of pretilt angle of liquid-crystal molecules has been extensively investigated [14,15,16]. These studies demonstrate that the pretilt angle of liquid-crystal molecules increases along with the rubbing strength [17,18]. In this thesis, the pretilt angle effect on LC device response time will be discussed in details.

### **1.5 Anchoring Energy**

LC directors close to the LC-substrate surfaces are strongly influenced by the surface alignment, and their orientation is different from those in the bulk region. The alignment effects of the boundaries are also transmitted to the bulk region. Therefore, the anchoring energy is an important property for an LC cell. It affects not only the LC alignment but also the electro-optic properties such as threshold voltage and response time. Compared with strong anchoring energy, weak anchoring leads to lower threshold, shorter rise time and longer decay time [19, 20].

The physical meaning of anchoring energy is the energy required for the maximum deviation of the director in the LC-substrate adjacent areas from the easy orientation position. Usually we have two types of anchoring: one is related to the deviation of the director from the normal to the substrate, which is called as the polar anchoring energy  $W_\theta$ ; and the other is related to the deviation in the plane of the substrate: the azimuthal anchoring energy  $W_\phi$ . For homogeneously-aligned and vertically-aligned liquid crystal, usually only the polar

anchoring energy  $W_\theta$  is considered. The  $W_\phi$  effect is usually important for TN, STN liquid crystal modes.

If the anchoring energy is considered, the total free energy of a nematic liquid crystal is written as follows:

$$F = \int_0^d \frac{1}{2} [K_{11} \cos^2 \phi + K_{33} \sin^2 \phi] \left(\frac{d\phi}{dz}\right)^2 dz + f_s(0) + f_s(d), \quad (1.13)$$

$$f_s = \frac{1}{2} W \sin^2 \theta, \quad (1.14)$$

where  $f_s$  is the surface anchoring energy densities of nematic liquid crystal. The integral term represents the bulk free energy density, and  $\phi$  is the angle between the LC director and the substrate rubbing direction,  $d$  is the cell gap. This important equation will be discussed again in the following chapters, and here we will only introduce the extrapolation length concept from these equations.

If we consider a liquid crystal cell with the same top and bottom alignment, Eq.(1.13) can be simplified to Eq.(1.15) using the “one-constant approximation” and “small angle approximation” [21]. Here we assume that  $K_{11}=K_{22}=K_{33}=K$  (one-constant approximation), therefore, we have [64].

$$F = \frac{1}{2} K \int_0^d \left(\frac{d\phi}{dz}\right)^2 dz + 2 f_s. \quad (1.15)$$

In equilibrium state the free energy is minimal and its variation  $\delta F$  is zero:

$$\delta F = 2[W\theta - K \frac{d\theta}{dz}] \delta\theta'_{z=0} - K \int_0^d \frac{d^2\theta}{dz^2} \delta\theta dz = 0. \quad (1.16)$$

Since  $\delta\phi$  is arbitrary, to satisfy the condition  $\delta F=0$ :

$$\frac{d^2\theta}{dz^2} = 0, \quad (1.17)$$

at  $z \sim d$  region,

$$W\theta - k \frac{d\theta}{dz} = 0. \quad (1.18)$$

The solution of Eq.(1.17) is  $\theta = az + b$ . Taking Eq.(1.18) into consideration, we have

$$\theta = \frac{W}{2K + Wd} (z + K/W). \quad (1.19)$$

Let  $\theta=0$ , we have

$$b = |z| = \frac{K}{W}, \quad (1.20)$$

where  $b$  has the dimension of a length, and is usually called as the *extrapolation length*.

Eq.(1.20) is a basic formula describing the interaction of the nematic liquid crystal with solid substrates.

Eq.(1.14) is the well-known Rapini-Papoular model, which was first introduced by A. Rapini and M. Papoular [22]. After that, pretilt angle was also taken into account, which leads to the following anchoring energy expression [23].

$$f_s = \frac{W}{2} \sin^2(\theta - \theta_0). \quad (1.21)$$

Generally speaking, the external applied voltage may reorient the twist and tilt angles of the surface LC directors. Then both the polar and azimuthal anchoring energies need to be considered. The polar anchoring energy  $W_p$  is related to the deviations of the surface tilt angle  $\theta$  from the pretilt angle  $\theta_0$ . The azimuthal twist angle  $\phi$  is deviated from the pretwist angle  $\phi_0$ , which is related to the azimuthal anchoring energy  $W_a$ . Therefore, we have:

$$f_s = \frac{1}{2} [W_p \sin^2(\theta - \theta_0) + W_a \sin^2(\phi - \phi_0)]. \quad (1.22)$$

This expression is widely employed as a generalization of the original Rapini-Papoular model. In this dissertation, vertically-aligned LC is mainly discussed, and the azimuthal

anchoring energy  $W_a$  is not involved, and we mainly use the expression Eq.(1.14),

$$f_s = \frac{1}{2} W \sin^2 \theta, \text{ in our studies.}$$

## **1.6 Thesis Overview**

The dissertation is organized as follows.

Chapter Two reviews the liquid crystal numerical simulation methods briefly. The simulation of anchoring energy effect is discussed, and the dynamic simulation of dual-frequency liquid crystal (DFLC) is compared with experimental results. We also investigate the phase retardation dependent LC response time using numerical simulation methods.

Chapter Three discusses a novel high-electric-field approach to characterize the anchoring energy of vertically-aligned liquid crystal cells.

In Chapter Four, anchoring energy and cell gap effects on liquid crystal response time is analyzed theoretically, and studied experimentally. Two different theoretical analysis approaches are employed to derive analytical expressions, and consistent results are obtained.

Chapter Five discusses the pretilt angle effect on liquid crystal response time. Analytical expressions are derived to quantitatively correlate the liquid crystal pretilt angle to its dynamic performance. Experimental results are also included to confirm our theoretical analysis.

Finally, in Chapter Six, the key achievements of this dissertation are summarized.

## CHAPTER TWO: NUMERICAL SIMULATION METHODOLOGIES

Numerical simulation is important for the design and optimization of LC devices. It can also be used to study physical effects which are hard to be investigated by experimental methods only, such as the anchoring energy effects. LC simulation methods are discussed in this chapter. In general, our liquid crystal simulation programs include two steps: (1) LC director distribution simulation, (2) optical simulation.

In this chapter, some simulation results are also discussed, including the simulation of anchoring energy effect, dynamic simulation of dual-frequency liquid crystal, and phase-retardation dependent LC response time effect.

### **2.1 Simulation of LC Director Distribution**

When no voltage is applied on an LC cell, the distribution of LC molecules in the cell is determined by the surface alignment. When the applied voltage exceeds the Freedericksz transition threshold voltage  $V_{th}$ , the LC molecules in the bulk of the cell will be reoriented by the external electric field.

For LC device simulation, the LC director distribution in external electric field needs to be solved first. Here we have two cases. One is to simulate the voltage dependent LC director distribution and optical response, which is called as *static state simulation*; the other one is *dynamic process simulation*, which is to simulate the time dependent LC director distribution and optical response. Both cases are discussed in this chapter.

Finite element method (FEM) is employed to develop our simulation programs. FEM is a well recognized numerical simulation method. A general purpose FEM computer program can be easily developed to rigorously analyze the problems where analytical solutions are difficult to obtain. The numerical simulation of LC device is based on the assumption that the LC system acts to minimize its free energy.

### 2.1.1 Static State Simulation

The *static state simulation* is to simulate the voltage dependent LC director distribution, which is then used to calculate the optical response. LC director distribution is decided by the balance of the torques between the elastic free energy and electric energy. To obtain the LC director distribution, the Gibbs free energy density  $f_g$  needs to be minimized.

$$f_g = f_s - f_e, \quad (2.1)$$

where the elastic free energy  $f_s$  of a liquid crystal system in terms of the director  $\mathbf{n}$  is given by

$$f_s = \frac{1}{2}K_{11}(\nabla \cdot \mathbf{n})^2 + \frac{1}{2}K_{22}(\mathbf{n} \cdot \nabla \times \mathbf{n})^2 + \frac{1}{2}K_{33}|\mathbf{n} \times \nabla \times \mathbf{n}|^2. \quad (2.2)$$

The expression for electric free energy  $f_e$  is:

$$f_e = \frac{1}{2}\mathbf{D} \cdot \mathbf{E} = \frac{1}{2}\varepsilon \nabla V \cdot \nabla V, \quad (2.3)$$

and  $\mathbf{E} = -\nabla V$ .  $V$  is the voltage distribution, and  $\varepsilon$  is the dielectric tensor of the LC cell. The relative dielectric tensor is given by [24]:

$$\boldsymbol{\varepsilon}_r = \begin{bmatrix} \varepsilon_{xx} & \varepsilon_{xy} & \varepsilon_{xz} \\ \varepsilon_{yx} & \varepsilon_{yy} & \varepsilon_{yz} \\ \varepsilon_{zx} & \varepsilon_{zy} & \varepsilon_{zz} \end{bmatrix}. \quad (2.4)$$

The total free energy  $F$  of the liquid crystal system is the integration of the free energy density  $f_g$ :

$$F = \iiint_V f_g dV . \quad (2.5)$$

By minimizing  $F$ , the voltage dependent LC director distribution is available.

In the FEM numerical simulation, boundary conditions are critical. Usually we consider that the LC directors on the substrate won't reorient in external electric field, that is, the anchoring energy  $W$  is infinity. Then the LC directors on the substrates are fixed at the pretilt angle  $\theta_p$  in the simulation program.

However, if the anchoring energy needs to be studied, the LC directors on the LC substrates are not fixed and their orientation will also change in external electric field, and the reorientation is dependent on  $W$ . Therefore, the total free energy  $F$  needs to include the anchoring energy terms, as discussed in Eqs.(1.13) and (1.14) before. The details simulation results will be discussed later in the chapter.

### 2.1.2 Dynamic Process Simulation

To simulate the time dependent LC director distribution, we solve the voltage distribution using the finite element method (FEM) first [25] and obtain the dynamic director distribution using the Finite-Difference Time-Domain Method (FDTD) [26].

The dynamic evolution of LC director  $n_i$  is obtained by the analysis of the electric and elastic properties of the LC material. The main idea is to use Euler-Lagrangian equations to

minimize the free energy. After applying the Gibbs free-energy density  $f_g$  in the Erickson-Leslie theory, we have [27]:

$$\gamma_1 \frac{dn_i}{dt} = -[f_g]_{n_i} + \lambda n_i, \quad i = x, y, z, \quad (2.6)$$

where  $\gamma_1$  is the rotational viscosity,  $n_i$  is Cartesian component of the director,  $\lambda$  is a Lagrange multiplier used to maintain the unit length of the director and  $[f_g]_{n_i}$  is the Euler-Lagrangian equations. However, an update formula of the LC director and the  $\lambda$  parameter can not be both obtained from this equation. So we drop the Lagrange multiplier term and simply renormalize the director after each iteration. The Euler-Lagrangian equations  $[f_g]_{n_i}$  are expressed as [27]:

$$[f_g]_{n_i} = \frac{\partial f_g}{\partial n_i} - \frac{d}{dx} \left( \frac{\partial f_g}{\partial n_i / dx} \right) - \frac{d}{dy} \left( \frac{\partial f_g}{\partial n_i / dy} \right) - \frac{d}{dz} \left( \frac{\partial f_g}{\partial n_i / dz} \right), \quad i = x, y, z. \quad (2.7)$$

With the known electric energy density  $f_e$  and elastic energy density  $f_s$ , the updated director components after each time step  $\Delta t$  can be derived from equation Eq.(2.6) as

$$n_i^{new} = n_i^{old} - \frac{\Delta t}{\gamma_1} [f_g]_{n_i}, \quad i = x, y, z. \quad (2.8)$$

After this update, the director must be renormalized to have a unit length. This renormalization also depends on the numerical time step  $\Delta t$ . Therefore, the setting time step will be critical to the calculation accuracy. At each time step, the director distribution is used to solve the electro-optic performance of the simulated LC device. After the LC director distribution is updated, the voltage distribution and the electric energy distribution must be updated to represent the changes of the voltage distribution. This iteration continues until

setting convergence criteria is reached. This is a good approach in reducing the computation time while maintaining a reasonable accuracy.

Anchoring energy significant influences LC dynamics and this topic will be discussed in Chapter Four in details. FEM numerical simulation program is developed to simulate this effect. If anchoring energy  $W \sim \infty$ , the LC directors on the substrates are fixed at the pretilt angle, which is the same as the static simulation case. But if  $W$  is finite, surface dynamic equation needs to be utilized as the boundary conditions in our simulation program, and the simulation results will be given in Chapter Four.

## **2.2 Optical Simulation**

Several approaches have been developed to simulate the optical transmittance/reflectance of LC devices, such as: 1) Berreman's 4 by 4 matrix method [28, 29, 30, 31] ; 2) the extended Jones matrix (2 by 2 matrix) [32, 33, 34, 35, 36]. Berreman's 4×4 Matrix approach takes into account the effects of the refraction and multiple reflections between adjacent layers [29] However, it needs lengthy calculations and it is generally employed only for the normal incidence. Many approximations of this method have been proposed. Yeh [32] and Lien's [34] extended Jones matrix methods were derived to generalize the 2×2 Matrix formulation to the oblique incidence.

### **2.3 Static Simulation of Anchoring Energy Effects on Electro-optic Response of LC Cells**

The boundary conditions are critical for LC devices' numerical simulation. If strong anchoring is assumed, the LC directors on the surfaces are fixed. However, if finite anchoring energy is considered in the simulation, the simple boundary conditions of strong anchoring are not valid. The free energy expression Eq.(1.13) needs to include the surface anchoring energy term  $f_w$  of both the bottom and top substrates, therefore,

$$f = f_s + f_w(0) + f_w(d) - f_e. \quad (2.9)$$

The numerical simulation results in Figure 2.1 show anchoring energy dependent VA LC electro-optic responses. If the same driving voltage is applied, an LC cell with weaker anchoring has larger phase retardation because of more LC director reorientation in the surface region. The simulation parameters are: 7  $\mu\text{m}$  LC cell gap;  $K_{11}=16.7$  pN,  $K_{22}=7.0$  pN,  $K_{33}=18.1$  pN,  $\varepsilon_{\parallel}=3.6$ ,  $\varepsilon_{\perp}=7.8$ ,  $\Delta\varepsilon= -4.2$ ,  $V_{\text{th}}=2.17$  V, Wavelength  $\lambda=633$  nm; and the pretilt angle is 2 degree.

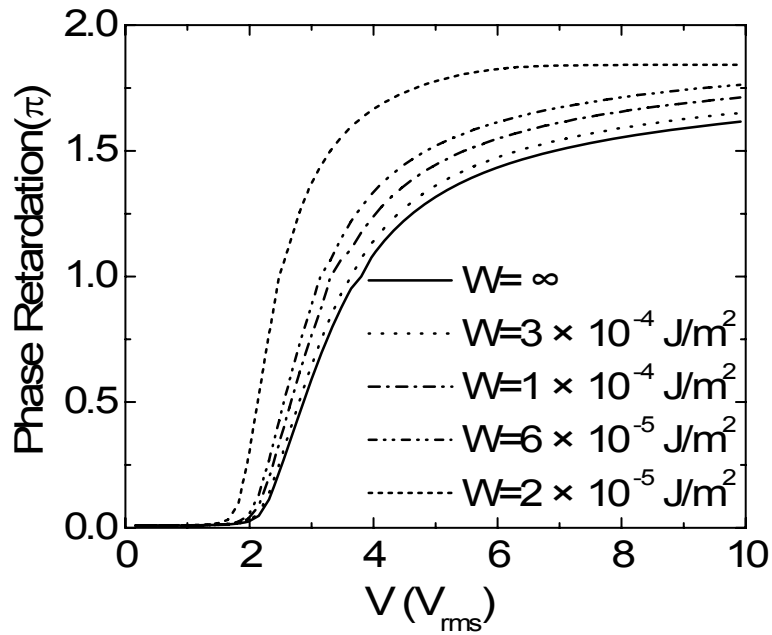


Figure 2.1: Anchoring energy  $W$  dependent electro-optic responses of a  $7 \mu\text{m}$  VA LC cell

Strictly speaking, the LC threshold voltage doesn't exist if the pretilt angle is nonzero, however, the threshold like behavior can be still observed, and here we still roughly consider it as threshold voltage of a LC device. From this figure, we notice that the threshold voltage is also dependent on anchoring energy  $W$ . Weaker anchoring energy leads to smaller threshold voltage, which is desired for low driving voltage and low power consumption of LC devices.

In the high applied voltage range ( $>6\text{V}$  in Figure 2.1), the LC directors in the bulk region of LC cell have been fully reoriented, and the reorientation of LC directors close to the surfaces will mainly contribute to the phase retardation changes. If the anchoring energy is weaker, the surface effect on LC cell phase change will be less important in the high applied voltage range, because the LC directors in surfaces region have been fully reoriented. As a result, if the

anchoring energy is weaker, the voltage-phase retardation curves are less steep, as shown in the high voltage range of Figure 2.1.

Both the anchoring energy effects on the threshold voltage and phase retardation have been studied extensively. In this dissertation, we develop an anchoring energy measurement method for VA liquid crystal cells, and it is discussed in Chapter Three. This measurement method is based on the anchoring energy effect on LC cell phase retardation in the high applied voltage range.

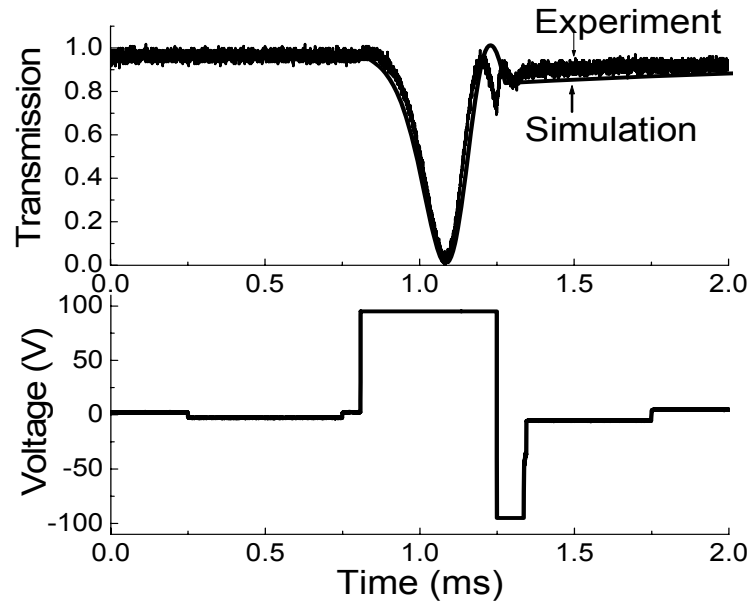
## **2.4 Dynamic Simulation of Dual-Frequency Liquid Crystal Device**

To further demonstrate the design function of our numerical simulation programs, we discuss dynamic simulation of a DF LC phase retarder. The simulation results are compared with experimental ones and they match very well [37].

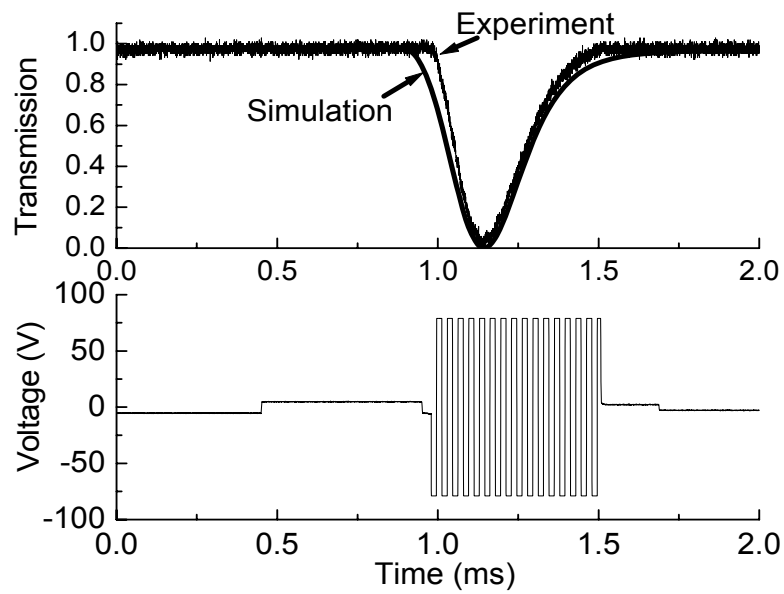
Most commercially available DF LC mixtures have low birefringence, high viscosity, and small  $|\Delta\varepsilon|$  values. To overcome these drawbacks, we prepared a high birefringence and low viscosity DF LC mixture using 30% biphenyl esters and 70% lateral difluoro tolanes. The physical properties of our DF LC mixture at room temperature ( $T=22^\circ\text{C}$ ) are as follows: cross-over frequency  $f_c \approx 4$  kHz,  $\Delta n = n_e - n_o = 0.25$  at  $\lambda=1.55$   $\mu\text{m}$ . In our experiments, 1 kHz low frequency and 30 kHz high frequency are chosen, where  $\Delta\varepsilon = 4.7$  at  $f = 1$  kHz and  $\Delta\varepsilon = -4.0$  at  $f = 30$  kHz. 9.2  $\mu\text{m}$  thick homogenous alignment cells are used and overdriving pulse voltages for both the rising and decay processes are decided for sub-millisecond response time.

In our DFLC phase retarder system, a  $2.5 V_{\text{rms}}$  bias voltage of 1 kHz, which is slightly less than the threshold voltage, is used to speed up the LC cell's response at rising process. An initial DFLC director distribution corresponding to the specific bias voltage is used to simulate its effect. The simulation shows that without the bias voltage, the rising time would be 0.7 ms longer under the same overdriving condition. As we know, the transmittance of such a phase retarder is  $I=I_0 \sin^2 [\delta/2]$ , where  $I_0$  is the incident light intensity,  $\delta$  is the phase retardation of the LC cell. The LC director reorientation thus can be revealed from the light transmission so that our simulation and experiments are correlated.

In the experiments, 1 kHz  $2.5 V_{\text{rms}}$  bias voltage and  $95 V_{\text{rms}}$  overdriving pulse are applied on the cell to reorient the LC directors. The overdriving voltage only lasts about 0.5 ms to avoid over-tilting. Then a  $5 V_{\text{rms}}$  low frequency (1 kHz) voltage is applied to hold the LC directors. The cell thus is kept at a  $2\pi$  phase retardation status before the high frequency voltage is applied. The detailed rising process is illustrated in Figure 2.2(a) and compared with the simulation result. The experimental curve matches well with the theoretical prediction. Both of them show a  $2\pi$  phase transition within less than 0.5 ms for this rising process. For the decay process, the LC directors are already tilted up, which is so called homeotropic state. A high frequency (30 kHz),  $79 V_{\text{rms}}$  voltage is used to drive the LC cell back to its original homogeneous distribution. From Figure 2.2(b),  $2\pi$  phase decay is achieved within only  $\sim 0.5$  ms, which also agrees well with our theoretical estimation.



(a) Rising process



(b) Decay process

Figure 2.2: Upper part of each figure shows the experiment result and simulation result, the under part shows the voltage and frequency modulation. Numerical simulation includes the dual frequency, overdriving and bias voltage effects, and it agrees well with the experimental results.

## **2.5 Simulation of Phase Retardation Dependent Liquid Crystal Electro-optic Modulation**

Liquid crystal optical response time was theoretically predicted to be dependent on LC device phase retardation by Wu [38]. The optical response time can be two or four times faster than LC directors' reorientation time  $\tau_0$ . In this part, the theoretical analysis is confirmed by experimental demonstration and numerical simulation. By applying sinusoidal driving voltage on a homogeneously-aligned LC cell, the frequency of the transient optical response ( $f_o$ ) is 2 or 4 times of  $f_e$ , where  $f_e$  is the frequency of sinusoidal driving voltage. If  $\delta_0$  is defined as the average phase retardation, the  $f_o=4f_e$  phenomenon exists when  $\delta_0 \sim N\pi$  ( $N$  is an integer), and  $f_o=2f_e$  if  $\delta_0 \sim (N-1/2)\pi$ .

In our experimental setup, a homogeneously aligned LC cell is placed between a pair of crossed polarizer and analyzer, and a He-Ne laser ( $\lambda=633\text{nm}$ ) is used as the light source. The optical transmittance is:

$$I = I_0 \sin^2\left(\frac{\delta_0}{2}\right), \quad (2.10)$$

where  $I_0$  is the incident light intensity, and  $\delta_0$  is the LC cell phase retardation. We use sinusoidal driving voltage in the experiments. Because the driving voltage is not a constant, the LC directors follow the transient driving voltage and reorient back and forth in the external electric field. Thus transient phase retardation shift  $\Delta\delta$  is observed around  $\delta_0$ .

From Eq.(2.10), if we only keep the second order of the Taylor expansion, it leads to

$$\begin{aligned}
\frac{I}{I_0} &= \sin^2\left[\frac{\delta_0 + \Delta\delta}{2}\right] = \frac{1}{2} - \frac{1}{2}\cos(\delta_0 + \Delta\delta) \\
&\approx \frac{1}{2} - \frac{1}{2}[\cos\delta_0 - \sin\delta_0 \cdot \Delta\delta - \frac{1}{2}\cos\delta_0 \cdot \Delta\delta^2 + \dots]. \\
&\approx \frac{1}{2}(1 - \cos\delta_0) + \frac{1}{2}\sin\delta_0 \cdot \Delta\delta + \frac{1}{4}\cos\delta_0 \cdot \Delta\delta^2
\end{aligned} \tag{2.11}$$

The transient phase shift  $\Delta\delta(t)$  can be correlated to the LC director response time  $\tau_0$  by the following equation [39],

$$\delta(t) \approx \delta_0 \exp(-2t/\tau_0), \tag{2.12a}$$

$$\Delta\delta(t) \approx \delta_0[1 - \exp(-2t/\tau_0)], \tag{2.12b}$$

which means that the phase response time is twice faster than the director's response time  $\tau_0$ .

If the phase retardation happens to be in the vicinity of  $\delta_0 \sim (N - \frac{1}{2})\pi$ , where N is an integer, substituting Eq.(2.12b) to Eq.(2.11), we find

$$\begin{aligned}
\frac{I}{I_0} &\approx \frac{1}{2}(1 - \cos\delta_0) + \frac{1}{2}\sin\delta_0 \cdot \Delta\delta + \frac{1}{4}\cos\delta_0 \cdot \Delta\delta^2 \\
&= \frac{1}{2}(1 - \cos\delta_0) + (-1)^{N+1}\delta_0[1 - \exp(-2t/\tau_0)]
\end{aligned} \tag{2.13}$$

From Eq.(2.13), the optical response time is 2X faster than the LC director response time  $\tau_0$ .

However, when the phase retardation is  $\delta_0 \sim N\pi$ , Eq.(2.10) can be reduced to

$$\begin{aligned}
\frac{I}{I_0} &\approx \frac{1}{2}(1 - \cos\delta_0) + \frac{1}{2}\sin\delta_0 \cdot \Delta\delta + \frac{1}{4}\cos\delta_0 \cdot \Delta\delta^2 \\
&= \frac{1}{2}(1 - \cos\delta_0) + (-1)^N \frac{\delta_0^2}{4} \cdot [1 - \exp(-2t/\tau_0)]^2 \\
&= \frac{1}{2}(1 - \cos\delta_0) + (-1)^N \frac{\delta_0^2}{4} \cdot [1 - 2\exp(-2t/\tau_0) + \exp(-4t/\tau_0)]
\end{aligned} \tag{2.14}$$

Under this condition, the optical response time can be up to 4X faster than  $\tau_0$ . Especially when  $t/\tau_0$  is small,  $I/I_0$  is mainly determined by the  $\exp(-4t/\tau_0)$  term because it decreases much faster than the  $\exp(-2t/\tau_0)$  term.

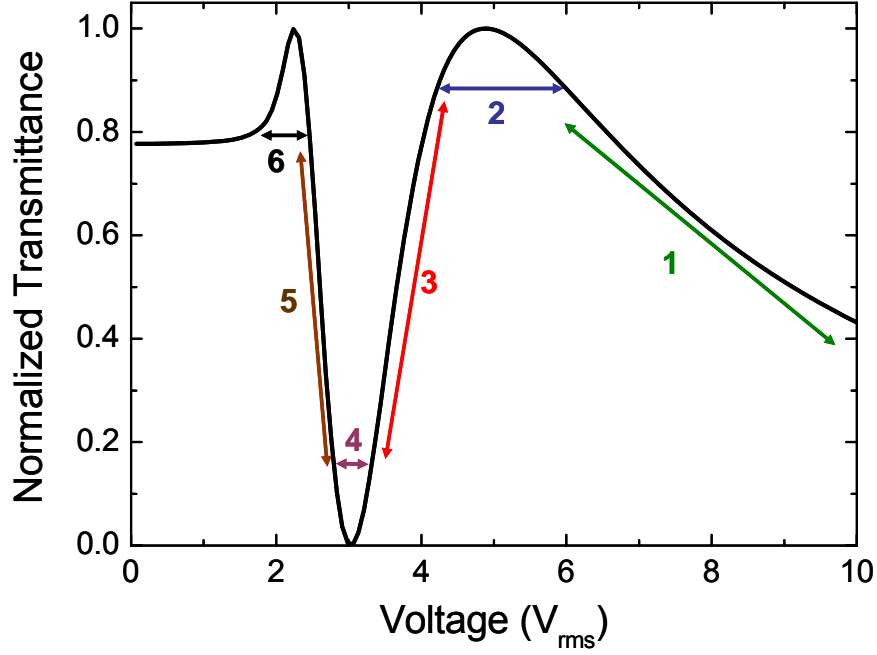


Figure 2.3: Voltage-dependent normalized transmittance of a homogeneous LC cell. Regions 2, 4, and 6 correspond to  $\delta_0 \sim N\pi$ , and regions 1, 3, and 5 correspond to  $\delta_0 \sim (N - \frac{1}{2})\pi$ .

Figure 2.3 is a plot of voltage-dependent normalized transmittance of a typical homogeneous LC cell. When  $\delta_0 \sim N\pi$ , the transmittance of the LC cell is either at a maximum (regions 2 and 6) or at a minimum (region 4). If we define  $f_p$  as the oscillation frequency of  $\Delta\delta$ , then  $f_o = 2f_p = 4f_e$  is predicted by our analytical results. If  $\delta_0 \sim (N - \frac{1}{2})\pi$ , that

is, the LC transmittance is around the regions 1, 3 and 5 in Fig. 2, the analytical results lead to  $f_o=f_p=2f_e$ .

To further study this transient effect, experimental results are used to demonstrate this effect, and FEM numerical simulation is employed to simulate the transient phase and optical response. The simulation results show that the LC directors' orientation fluctuates in external sinusoidal electric field, and it results in a small phase shift  $\Delta\delta$  around  $\delta_0$ . Then optical "ripples" are induced by  $\Delta\delta$ . The LC material we used has the following parameters:  $K_{11}=11.7\times 10^{-12}$  pN,  $K_{22}=8.8\times 10^{-12}$  pN,  $K_{33}=19.5\times 10^{-12}$  pN,  $\Delta\varepsilon=2.8$ , and  $\Delta n=0.21$  at  $\lambda=633$ nm,

This  $f_o=2f_p=4f_e$  effect is experimentally demonstrated in Figure 2.4. Numerical simulation results in Figure 2.5 also confirm our theoretical analysis and experimental results.

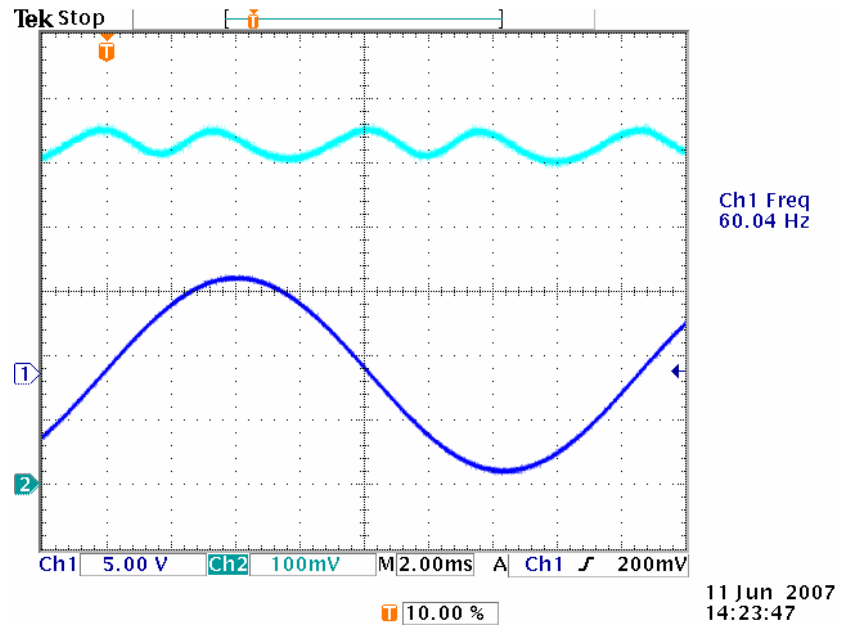


Figure 2.4: Experimental demonstration of  $f_o=4f_e$  at  $f_e=60\text{Hz}$ . The applied voltage  $V_{pp}=14.87$  V and  $\delta_0$  is around  $1\pi$ .

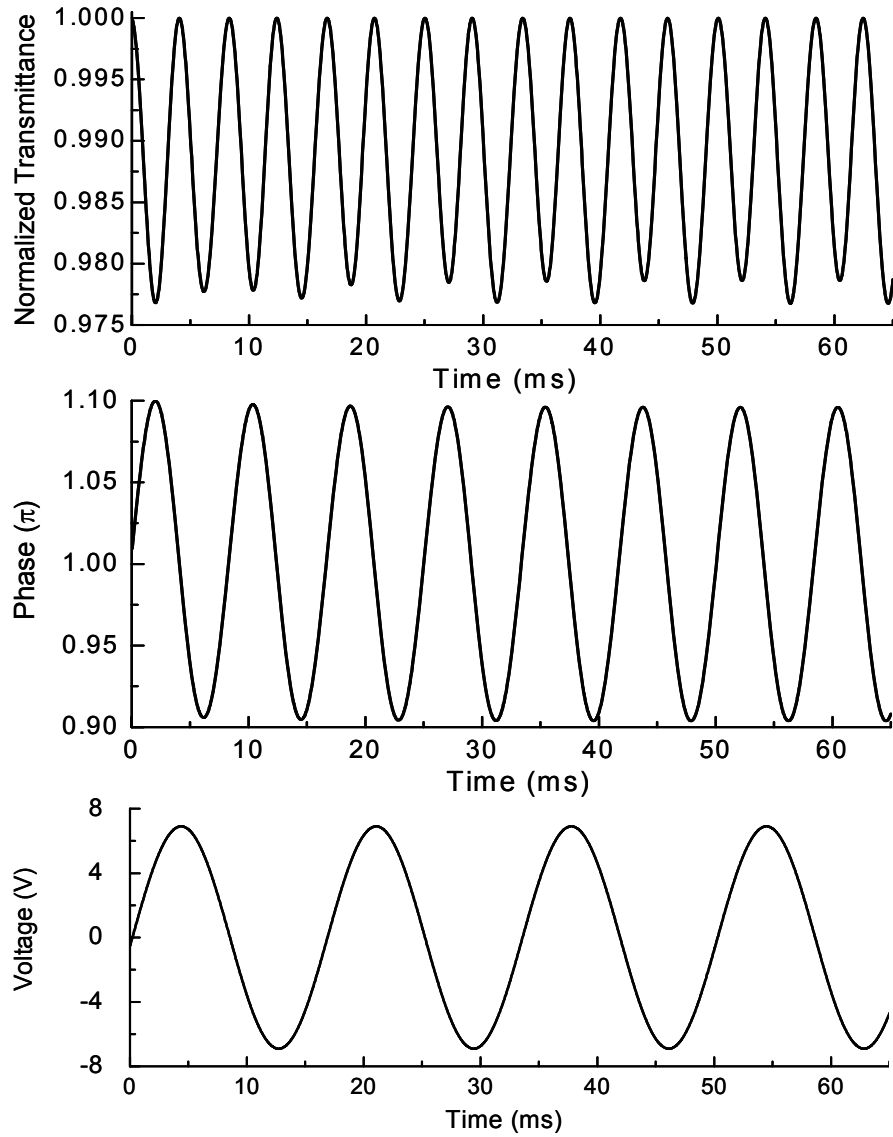


Figure 2.5: Simulation results of  $f_o=2f_p=4f_e$ , where  $f_e=60\text{Hz}$ . In the simulation,  $V_{pp}=13.8\text{ V}$  is used to keep  $\delta_0\sim\pi$ , and peak-to-peak phase shift  $\Delta\delta\sim 0.19\pi$ . Then  $f_o=4f_e$  because the  $\Delta\delta$  exists at the maximum point of optical transmittance, that is, around region 2 in Figure 2.3.

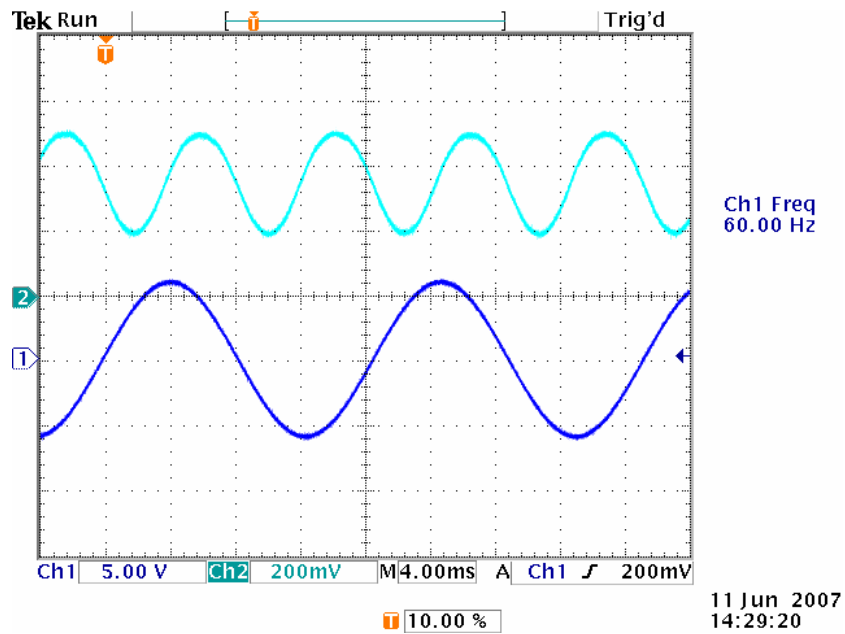


Figure 2.6: Experimental demonstration of  $f_o=2f_e$  and  $f_e=60\text{Hz}$ . The peak-to-peak driving voltage  $V_{pp}=11.81\text{ V}$  and  $\delta_0\sim 1.5\pi$ .

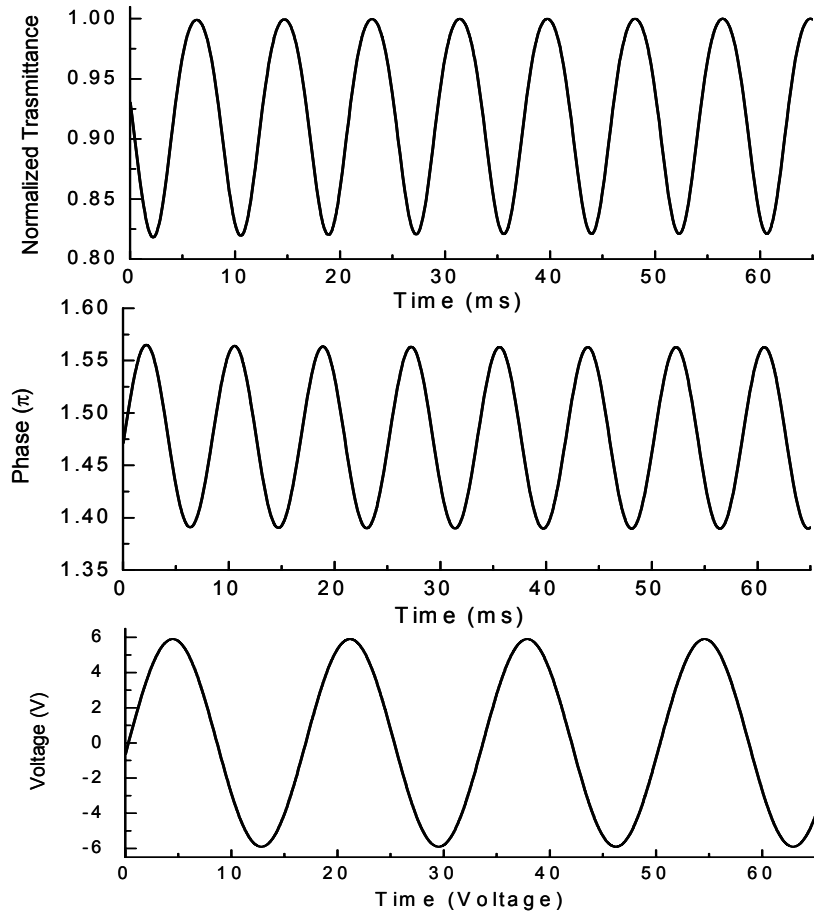


Figure 2.7: Simulation results of  $f_o=2f_e$ , and  $f_e=60$  Hz. In the simulation,  $V_{pp}=11.80$  V is used to keep  $\delta_0 \sim 1.5\pi$ , which is around region 2 of Figure 2.3. The  $\Delta\delta$  peak-to-peak amplitude is  $0.17\pi$ .

The observed transient phenomena are mainly determined by the dynamic driving voltage. The transient LC dynamic process is decided by the balance between the elastic and electric energy density. The sinusoidal driving voltage is changing continuously and is applied on LC cells as a bias voltage. When the transient driving voltage decreases from its peak amplitude, LC directors relax accordingly as the bias voltage decreases. Once the decreasing cycle of voltage amplitude is finished, the driving voltage amplitude starts to increase. The increasing bias voltage reorients the LC directors back, even if the LC directors don't fully decay from the previous cycle yet. Therefore, the LC directors are consistently driven by the external electric field and they must follow the cycles of sinusoidal driving voltage. Since the sinusoidal driving voltage is changing continuously, a simple analytical solution is not available. Numerical simulation is used to calculate the transient phase shift. The simulation shows that, at a lower driving frequency, the longer period allows more time for LC directors' reorientation, which leads to a larger  $\Delta\delta$  and more significant LC cell transmittance fluctuation. The frequency of the driving voltage also influences  $\Delta\delta$ . The driving frequency of a thin-film-transistor (TFT) LCD is typically at 60-120 Hz, thus, the transient optical fluctuation may influence the grayscales of the display device.

This phenomenon is general for nematic liquid crystal materials. Both our experiments and simulation show that a higher birefringence LC material causes a larger  $\Delta\delta$  under the same driving condition. The voltage amplitude is another factor affecting  $\Delta\delta$ . According to our simulation, larger voltage amplitude induces a more noticeable LC director deformation

which, in turn, results in a larger  $\Delta\delta$ . And finally the total phase retardation ( $\delta_0$  and  $\Delta\delta$ ) jointly determines the transient optical transmittance of the LC cell.

In this part, we mainly discuss the sinusoidal driving voltage condition. However, this LC dynamic process can be generalized to other driving conditions, as long as a transient phase shift is induced by an external driving voltage. In our experiments, various voltage waveforms (rectangular and triangular) were used and similar results were observed.

## **CHAPTER THREE: POLAR ANCHORING ENERGY MEASUREMENT**

### **3.1 Introduction**

Anchoring energy is an important parameter for an LC cell because it affects not only the LC alignment but also the electro-optic properties such as threshold voltage and response time. Various experimental techniques have been developed for measuring the anchoring energy. These methods can be categorized into two camps: field-on and field-off, depending on whether an external field is applied or not. Examples of the field-off methods are the wedge cells technique [40] and the light scattering technique. [41] In the field-on approaches, both electric field [42,43] and magnetic field [44] techniques have been considered. The field-on techniques are based on the measurements of the LC dielectric or diamagnetic Fredericksz transition effects. Usually, a strong electric field is more easily accessible and practical than a magnetic field. For this reason, the high-electric-field technique [42] is most commonly employed for measuring the polar anchoring energy. Afterward, a modified electric field technique was suggested for measuring the anchoring energy of some homogeneous cells. [43,45]. However, some inconsistent results have been reported by different research groups that have used even the same alignment method and LC material, mainly because of the complexity of the LC anchoring energy measurement.

In a VA cell, the liquid crystal molecules are aligned nearly perpendicular to the substrate surfaces. Under crossed polarizer/analyzer configuration, the VA cell exhibits an excellent contrast ratio. At normal incidence, the device's contrast ratio is insensitive to light

wavelength, LC layer thickness, and operating temperature. Because of these attractive features, VA cells have been used extensively for direct-view and projection displays. The performance of a VA cell depends on the anchoring interaction between the LC monolayer and the surface alignment layers. Substrate surface treatment and the surfactant play crucial roles for achieving a uniform pretilt angle. Good molecular alignment in a VA cell is usually more difficult to obtain than that in a homogeneous cell.

So far, only a few experimental methods have been developed for characterizing the anchoring energy of VA cells because of the complexity in theory and experimental technique. [46] The performance of a VA-LCD strongly depends on the effective control of surface treatment, therefore it is essential to develop a simple and reliable technique for measuring the anchoring energy of VA LC cells.

In this Chapter, a reliable electric field technique for measuring the anchoring energy of VA cells is developed. Firstly, we briefly introduce the anchoring energy measurement method by the Freedericksz transition method, which is applicable on VA LC cells. In Section 3.3, we derive the theoretical expressions which lay down the foundation for the experimental techniques. In Section 3.4, we perform confirming experiments and obtain the anchoring energy data for various VA LC cells. These results are useful for understanding the basic surface interaction mechanisms between the LC molecules and the alignment agents. Using this practical technique, we can select a proper alignment method to improve the VA-LCD performance.

### **3.2 Theory of Anchoring Energy Measurement by Freedericksz Transition**

As mentioned previously, the Freedericksz transition of an LC cell is influenced by anchoring energy of both the top and bottom substrates. Weaker anchoring energy usually leads to smaller threshold voltage, as shown in the simulation results of Figure 2.1. Therefore, the anchoring energy can be determined from the LC threshold voltage measurement if the correlation between them is known. Strictly speaking, LC threshold voltage doesn't exist if pretilt angle is not zero. But the LC threshold voltage still exists for LC cells with finite anchoring energy, if the pretilt angle can be ignored.

In [47], the relationship between the anchoring energy and threshold voltage is given by:

$$\operatorname{ctg}\left[\pi \frac{V_{th}(W)}{V_{th}(\infty)}\right] = \frac{\pi K V_{th}(W)}{W d V_{th}(\infty)},$$

where the elastic constant  $K$  is dependent on the LC deformation, that is, splay, bend or twist.

$V_{th}(W)$  and  $V_{th}(\infty)$  are the threshold voltage when the polar anchoring energy is finite and infinite, respectively. When  $W$  is relatively large, the above equation can be simplified to:

$$V_{th}(W) = V_{th}(\infty) \left(1 - \frac{2K}{Wd}\right).$$

These two equations correlate  $W$  with the threshold voltage  $V_{th}$ , which is useful for the anchoring energy measurement. However, pretilt angle also significantly influences the “threshold” like behavior of LC cell, which might smear the anchoring energy effect on LC threshold voltage and leads to inaccurate measurement results.

### 3.3 Theory of Anchoring Energy Measurement by High-Electric-Field Method

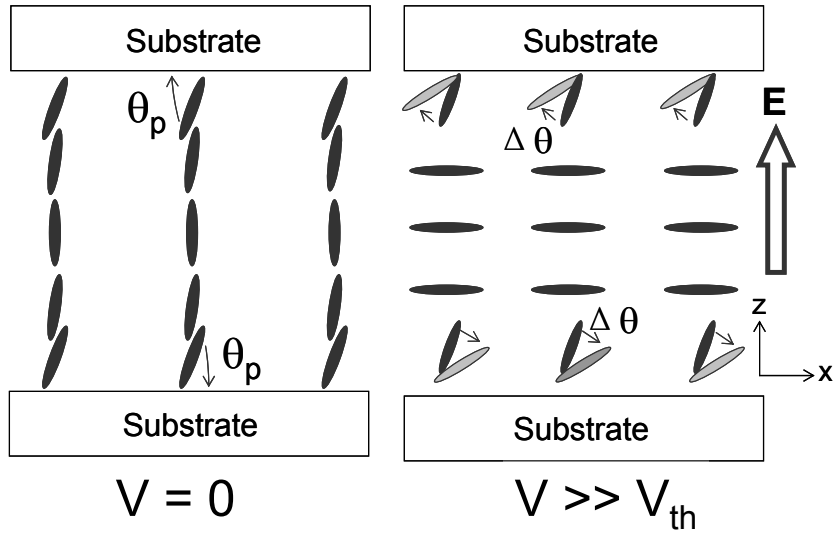


Figure 3.1: Schematic drawing of the LC director distribution of a VA cell. Left:  $V=0$  and right:  $V \gg V_{th}$ . The LC directors near the substrate surfaces could be reoriented when  $V \gg V_{th}$ , and the reorientation depends on the anchoring energy  $W$ .

Figure 3.1 shows the vertical alignment of nematic LC molecules confined between two identical electrodes located at  $z = 0$  and  $z = d$ . Without external electric fields, the pretilt angle  $\theta_p$  is close to  $\pi/2$ , which defines the minimum surface anchoring potential of LC directors on the substrates. Once the applied voltage exceeds a threshold, the LC directors are reoriented in the  $x-z$  plane. The LC molecules near the substrate surfaces are usually considered as *hard* anchored in most theoretical analysis. However in reality, these boundary layers will also rotate and make a small contribution to the overall phase retardation if the

external field is sufficiently high. In a specific voltage range, we find that the anchoring energy can be extracted through the simple phase retardation measurement.

Our goal is to determine anchoring energy from the LC director response to the external electric field. In theory, the LC director distribution profile can be obtained by minimizing the free energy of the cell. In a voltage-on state, let us assume that the LC directors are reoriented uniformly in the  $x$ - $z$  plane and both substrates are treated identically, the free energy per unit area of the VA LC cell can be written as

$$F = \int_0^d \frac{1}{2} [K_{11} \cos^2 \phi + K_{33} \sin^2 \phi] \left( \frac{d\phi}{dz} \right)^2 - D \cdot E dz + f_s(0) + f_s(d). \quad (3.1)$$

The integral term in Eq.(3.1) represents the bulk free energy density where  $K_{11}$  and  $K_{33}$  are the splay and bend elastic constants, respectively,  $\phi$  is the angle between the LC director and the substrate rubbing direction ( $x$ -axis),  $d$  is the cell gap, and  $D \cdot E / 2$  denotes the electric free energy density. The last two terms  $f_s(0)$  and  $f_s(d)$  represent the anchoring energy density on the bottom and top boundaries. From Rapini-Papoular model,  $f_s(0)$  and  $f_s(d)$  can be represented by,

$$f_s = \frac{1}{2} W \sin^2(\theta - \theta_p), \quad (3.2)$$

provided that the electric field-induced surface LC reorientation is not too far from the initial pretilt angle, i.e.,  $\Delta\theta = \theta - \theta_p$  is small; where  $\theta = \phi(0) = \phi(d)$  is the surface LC director orientation in a voltage-on state, and  $\theta_p$  is the pretilt angle, and  $W$  is the anchoring strength coefficient, also called as ‘‘anchoring energy’’. When  $\Delta\theta$  is small, e.g.,  $\Delta\theta < 0.3$  radian,

$\sin(\Delta\theta) \sim \Delta\theta$  and Eq.(3.2) can be simplified to  $f_s = \frac{1}{2}W(\Delta\theta)^2$ . The requirement of small  $\Delta\theta$  imposes that  $V \leq V_{\max}$ ; the maximum voltage  $V_{\max}$  is found to be proportional to the product of  $(\Delta\theta Wd)$  [45]. Since  $\Delta\theta$  cannot be too large, a larger  $Wd$  value would allow us to obtain a higher  $V_{\max}$ . If a VA cell has a weak anchoring strength (i.e., small  $W$ ), then we should use a thick cell gap in order to improve the measurement accuracy. For display devices, their cell gap is usually thin ( $d < 5 \mu\text{m}$ ), but their surface anchoring is strong. As a result, a thin display cell can still be used for the anchoring energy measurement.

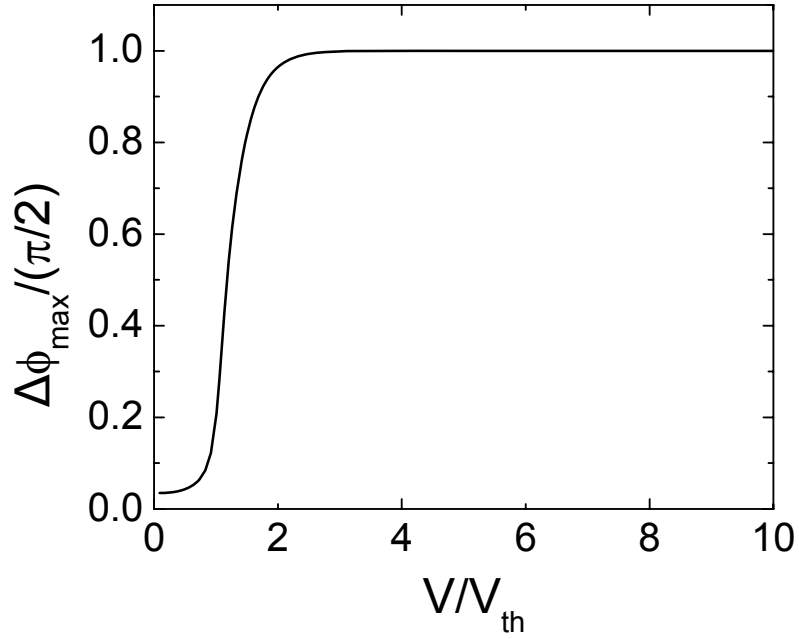


Figure 3.2: Numerical simulation for the voltage dependent  $\Delta\phi_{\max}$ , which validates the assumption of  $\Delta\phi_{\max} \approx \pi/2$  when  $V > 4V_{\text{th}}$ . The LC mixture used for simulation is Merck MLC-6608:  $K_{11}=16.7$  pN,  $K_{33}=18.1$  pN,  $\varepsilon_{\parallel}=3.6$ ,  $\varepsilon_{\perp}=7.8$ ,  $\gamma_1=0.186$  Pas,  $n_o=1.475$ , and  $n_e=1.558$ .

In the high electric field regime, the LC directors in the middle layer are fully reoriented, that is  $(\Delta\phi)_{\max} \sim \pi/2$ . Under this condition, the LC cell can be treated as semi-infinite plane during mathematical derivations. Figure 3.2 plots the numerical simulation of the voltage dependent  $(\Delta\phi)_{\max}$ . From Figure 3.2, the assumption  $(\Delta\phi)_{\max} \sim \pi/2$  is valid only when  $V$  is approximately  $\geq 4V_{th}$ . This implies that during anchoring energy experiment the applied voltage should exceed a minimum voltage  $V_{\min}$  which is 4X of the threshold voltage. From the above analyses, the anchoring energy can be extracted only in a specific voltage range:  $4V_{th} \leq V \leq V_{\max}$ .

From Eq.(3.1), by using the variational calculus, the Euler-Lagrange equation for a VA LC cell can be written as:[42]

$$\frac{d}{dz} \left[ (K_{11} \cos^2 \phi + K_{33} \sin^2 \phi) \left( \frac{d\phi}{dz} \right)^2 - \frac{D^2}{\epsilon_0 (\epsilon_{\parallel} \sin^2 \phi + \epsilon_{\perp} \cos^2 \phi)} \right] = 0. \quad (3.3)$$

And at  $z=0$ ,

$$\frac{df_s(\theta)}{d\theta} = (K_{11} \cos^2 \theta + K_{33} \sin^2 \theta) \frac{d\phi}{dz} \Big|_{z=0}, \quad (3.4)$$

which represents the torque balance at the LC-substrate interface.

For a normally incident beam with wavelength  $\lambda$ , the phase retardation  $R$  of the LC cell can be calculated as follows:

$$R = \frac{2\pi}{\lambda} \int_0^d [n_{eff} - n_o] dz. \quad (3.5)$$

In Eq.(3.5),  $n_{eff} = n_o / (1 - \nu \cos^2 \phi)^{1/2}$  and  $\nu = (n_e^2 - n_o^2) / n_e^2$ ; where  $n_o$  and  $n_e$  are the refractive indices of the ordinary and extraordinary rays, respectively.

Based on the above mentioned approximations, i.e., small  $\Delta\theta$  and  $(\Delta\phi)_{\max} \sim \pi/2$ ,

we derive the following linear equation for a VA LC cell with a pretilt angle  $\theta_p \approx \pi/2$ :

$$\frac{R}{R_0} = -\frac{1}{CV} \frac{\xi}{\Delta n} I(b, \gamma, \nu, \frac{\pi}{2}) + (1 + \frac{2K_{33}}{Wd}), \quad (3.6)$$

where  $\xi = (\frac{\varepsilon_0 \varepsilon_{\perp} S}{d}) \pi \sqrt{\frac{K_{33}}{\Delta\varepsilon}}$ , and

$$I(b, \gamma, \nu, \theta) = \frac{2}{\pi} \int_0^{\theta} \frac{1 - \nu + (1 - \nu)^{1/2}}{1 - \nu \cos^2 \phi + (1 - \nu \cos^2 \phi)^{1/2}} \times \frac{(1 + k \cos^2 \phi)^2 (1 + b \sin^2 \phi)^{1/2}}{\sin \phi} d\phi.$$

In Eq.(3.6),  $R_0$  is the maximum phase retardation of the VA cell,  $R/R_0$  is the normalized phase retardation,  $C$  is the LC cell capacitance which is dependent on the applied voltage  $V$ ,  $\Delta n = n_e - n_o$  is the LC birefringence,  $\Delta\varepsilon$  ( $<0$ ) is the dielectric anisotropy of the negative LC material,  $\varepsilon_{\perp}$  is the dielectric constant perpendicular to the LC directors,  $S$  is the electrodes area of the LC cell,  $k = (K_{11} - K_{33})/K_{33}$ , and  $b = (\Delta\varepsilon)/\varepsilon_0 \varepsilon_{\perp} < 0$ . The term  $\frac{\xi}{\Delta n} I(b, \gamma, \nu, \frac{\pi}{2})$  can be treated as a constant since all the related parameters are independent of voltage. In Eq.(3.6),  $R/R_0$  is expected to be a linear function of  $1/CV$  in a specific voltage regime. Through a linear fitting in this voltage range, the anchoring energy  $W$  can be determined from the intercept at  $(1/CV) \rightarrow 0$ .

Multiplying both sides of Eq.(4.6) by  $(CV)$ , we derive:

$$(\frac{R}{R_0} - 1)(CV) = \frac{2K_3}{Wd} (CV) - \frac{\xi}{\Delta n} I(b, \gamma, \nu, \frac{\pi}{2}). \quad (3.7)$$

If we plot  $(\frac{R}{R_0} - 1)(CV)$  as a function of  $(CV)$ ,  $W$  can be determined from the slope of

the curve, provided that  $K_{33}$  and  $d$  are known. As will be shown below, Eq.(3.7) is easier to fit than Eq.(3.6), because the voltage range for a linear fitting is more obvious. Please note

that Eqs.(3.6) and (3.7) are valid only in the  $V_{\min} \leq V \leq V_{\max}$  region, as mentioned previously.

In Eqs.(3.6) and (3.7), the LC cell capacitance  $C$  is also dependent on the LC director distribution and the applied voltage  $V$ . It is known that near the electrode edges, fringing field-induced LC reorientation is slightly different from that in the bulk. However, in most experiments the electrode area is large ( $>1 \text{ cm}^2$ ) so that the fringing field-induced LC deformation can be ignored. In the high voltage regime, the LC cell capacitance is not a constant. Rather, the product of  $CV$  is a linear function of  $V$  [1,48]:

$$CV = C_{\infty}(V - V'), \quad (3.8)$$

where  $C_{\infty}$  is the VA LC cell capacitance at  $V \rightarrow \infty$ , This equation predicts that the plot of  $(CV)$  against  $V$  is a straight line (with slope  $C_{\infty}$ ) when  $V \gg V_{th}$ . For a VA cell, the  $V'$  in Eq.(3.8) is related to the threshold voltage as:

$$V' = \alpha \left(1 - \frac{\epsilon_{\parallel}}{\epsilon_{\perp}}\right) V_{th}, \quad (3.9)$$

where  $\alpha = \frac{1}{\pi} \int_0^1 \sqrt{\frac{(1+r)(1+kx)}{x(1+rx)}} dx$ , and  $r = \frac{\epsilon_{\perp}}{\epsilon_{\parallel}} - 1$ .

If the LC material parameters are known,  $V'$  can be calculated easily and the undesired capacitance measurement can be avoided through adopting Eq.(3.8). Under such a circumstance, Eq.(3.7) can be simplified to

$$\left(\frac{R}{R_0} - 1\right)(V - V') = \frac{2K_{33}}{Wd}(V - V') - \frac{\xi}{C_{\infty}\Delta n} I(b, \gamma, \nu, \frac{\pi}{2}). \quad (3.10)$$

The anchoring energy is accessible through a linear fitting of the above equation.

### 3.4 Experiment

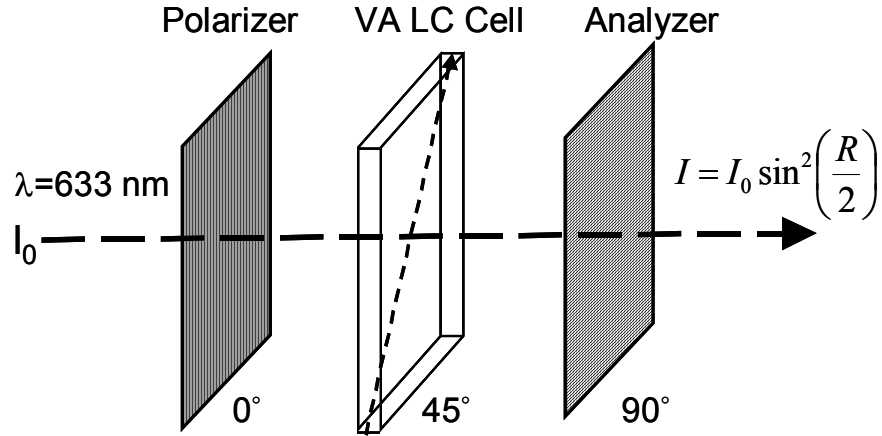


Figure 3.3: Experimental setup for measuring the anchoring energy of VA cells. A VA cell is placed between crossed polarizer and analyzer. The optical axis of the VA cell is oriented at  $45^\circ$  with respect to the polarizer.

Figure 3.3 depicts the experimental setup for measuring the anchoring energy of a VA cell. The LC cell is placed between a pair of crossed polarizer and analyzer. The optical axis of the cell is oriented at  $45^\circ$  with respect to the polarizer. The output transmittance is measured by a computer controlled LabVIEW data acquisition system. The transmittance of such a cell can be expressed as

$$I = I_0 \sin^2\left(\frac{R}{2}\right), \quad (3.11)$$

where  $I_0$  is the incident light intensity. The experiments are carried out at room temperature ( $T \sim 22^\circ\text{C}$ ) and  $\lambda=633 \text{ nm}$ . From the light transmittance measurement, the LC director profile

and phase retardation can be obtained and the anchoring energy extracted, as described below.

In our studies, various VA cells and negative LC materials are measured. To illustrate the measurement processes, we only show the experimental results of a 7.0  $\mu\text{m}$  buffed polyimide VA cell filled with Merck MLC-6608 negative LC mixture. In the first step, we measure the light transmittance of the VA cell and obtain the voltage dependent phase retardation. For a VA cell, the maximum phase retardation  $R_o$  cannot be accessed accurately by simply increasing the voltage because the boundary layers are impossible to be reoriented completely even at a high voltage. Thus, the extrapolation method [10] needs to be employed in order to obtain  $R_o$ . For the tested 7.0- $\mu\text{m}$  MLC-6608 VA cell,  $R_o$  is found to be  $1.982\pi$ . In the second step, we measure the voltage dependent LC cell capacitance using a computer-controlled Displaytech APT-III instrument. Figure 3.4 depicts the measurement results. Indeed, the measured capacitance results confirm that  $CV$  is linearly dependent on  $V$  in the high voltage region, as described by Eq.(3.8). Through a linear fitting in the high voltage region, an intercept of 1.24 V is obtained at  $CV=0$ .

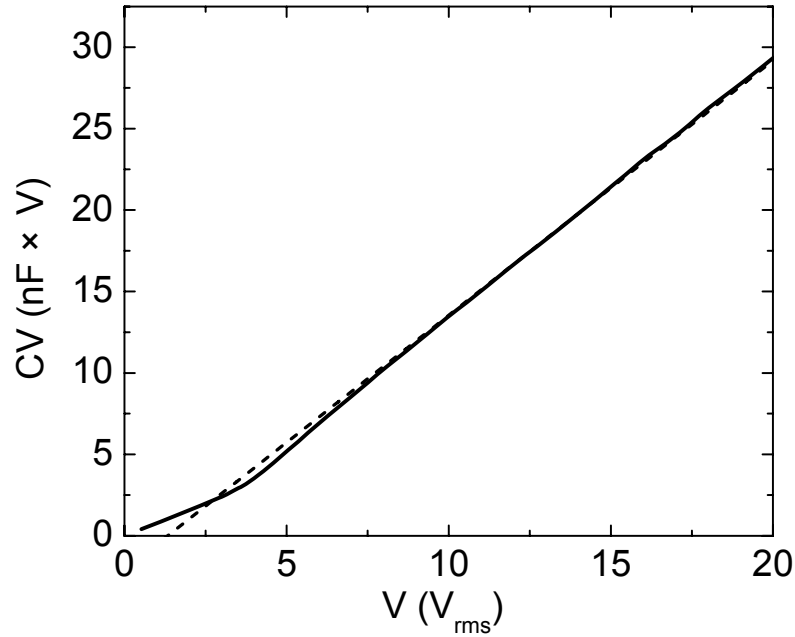


Figure 3.4: Voltage-dependent  $CV$  curve of a  $7 \mu\text{m}$  VA cell filled with MLC-6608. In the high voltage region, a linear curve is observed and the intercept at  $CV=0$  is  $1.24 V_{\text{rms}}$ .

Figure 3.4 plots  $R/R_o$  as a function of  $(1/CV)$ , according to Eq.(3.6). A linear curve is observed between 8 and 20  $V_{\text{rms}}$ . The projected intercept at  $1/CV = 0$  is 1.017, which leads to an anchoring strength of  $W=(3.0\pm 0.2)\times 10^{-4} \text{ J/m}^2$ . This extrapolation method works reasonably well in theory and the obtained results are accurate in some cases. However, this intercept extrapolation method has two disadvantages: the intercept is usually too close to 1 and the linearity exists only in a specific voltage regime. At a high voltage, the possible nonlinear behavior of the function is masked in appearance by the reciprocal  $(1/CV)$ . These two factors limit the accuracy of this method.

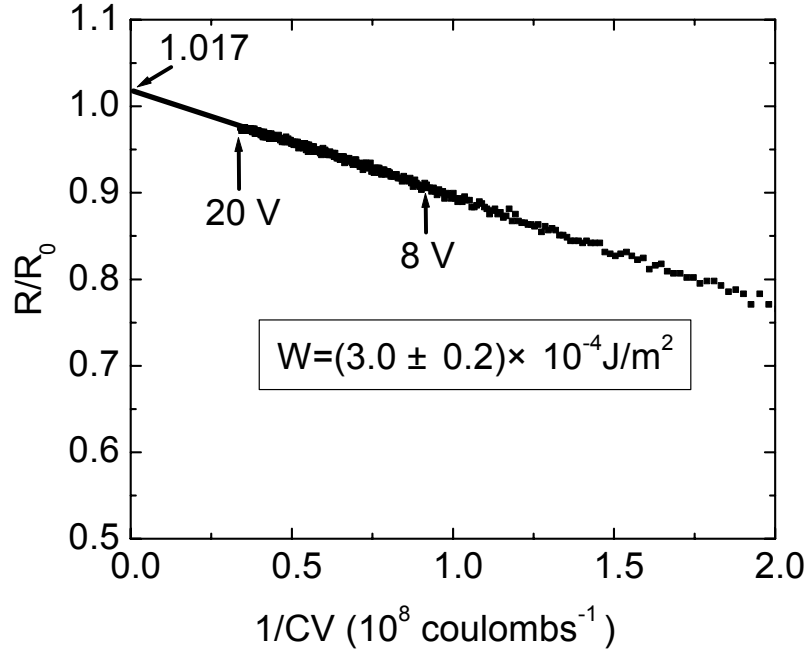


Figure 3.5: Illustration of the intercept extrapolation method described in Eq.(3.6). A linear fitting is obtained in the  $V > 8 V_{\text{rms}}$  region. The intercept at  $I/CV=0$  leads to  $W=(3.0 \pm 0.2) \times 10^{-4} \text{ J/m}^2$ . A  $7 \mu\text{m}$  VA cell filled with MLC-6608 is used as an example.

To find an easier and more reliable fitting process, we develop a slope fitting method. The variable  $(CV)$  would enable a more obvious fitting voltage range than  $I/(CV)$ . Figure 3.5 plots the measured  $(R/R_o - 1)$  as a function of  $CV$ , according to Eq.(3.7). The result shows that a good linear fitting is obtained between  $9$  and  $18 V_{\text{rms}}$ . By fitting the slope of the linear curve, an anchoring strength of  $W=(3.1 \pm 0.2) \times 10^{-4} \text{ J/m}^2$  is deduced. The threshold voltage of MLC-6608 LC material is  $V_{\text{th}} \sim 2.14 V_{\text{rms}}$ , which gives a minimum voltage of  $V_{\text{min}} = 4V_{\text{th}} \sim 8.56$

$V_{\text{rms}}$ . From our theoretical analyses shown in Sec. II, a linear curve is predicted in the  $4V_{th} \leq V \leq V_{\text{max}}$  range. This prediction is validated as observed from Figure 3.6.

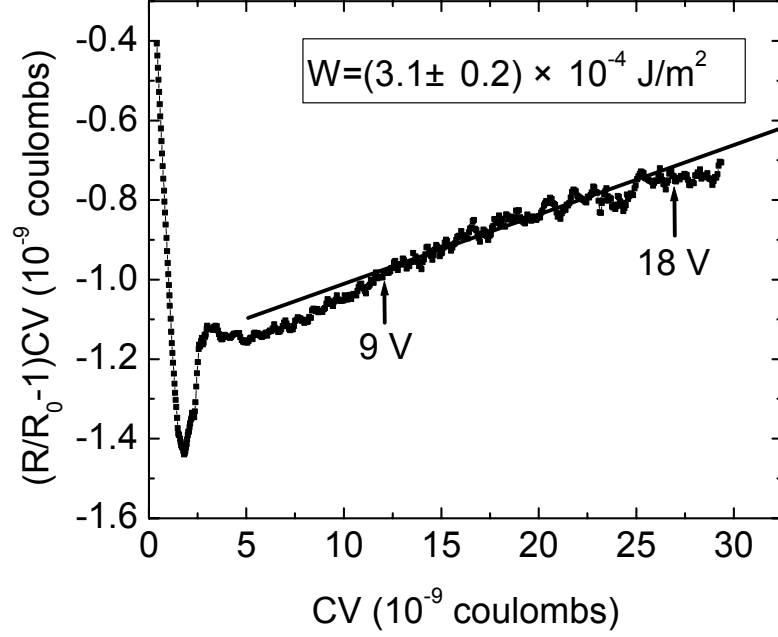


Figure 3.6: Illustration of the slope fitting method according to Eq.(3.7). A linear fitting between  $V=9 V_{\text{rms}}$  and  $18 V_{\text{rms}}$  is observed, and the anchoring energy is deduced as  $W=(3.1 \pm 0.2) \times 10^{-4} \text{ J/m}^2$ . A  $7 \mu\text{m}$  VA cell filled with MLC-6608 is tested as an example.

For accurate determination of anchoring energy, the voltage dependent LC cell capacitance should be taken into consideration. However, in-situ capacitance measurement can be tedious and time consuming. We could use an analytical form of the voltage-dependent capacitance, instead of using the actual experimental data. Eq.(3.10)

provides a convenient method for measuring  $W$  without the variable  $C$ . For the  $7.0\ \mu\text{m}$  VA cell,  $V'$  is calculated to be  $0.96\ \text{V}$ , which is close to the  $1.24\ \text{V}$  deduced from Figure 3.4. Our results in Figure 3.7 show that the curve is less linear than that shown in Figure 3.6. The obtained anchoring strength  $W=(3.2\pm 0.3)\times 10^{-4}\ \text{J/m}^2$  is  $\sim 3\%$  higher than that obtained from Figure 3.6. Although this alternative method mentioned in Eq.(3.10) can skip the cell capacitance measurement, it is somewhat less accurate because the theoretical instead of experimental capacitance value is used.

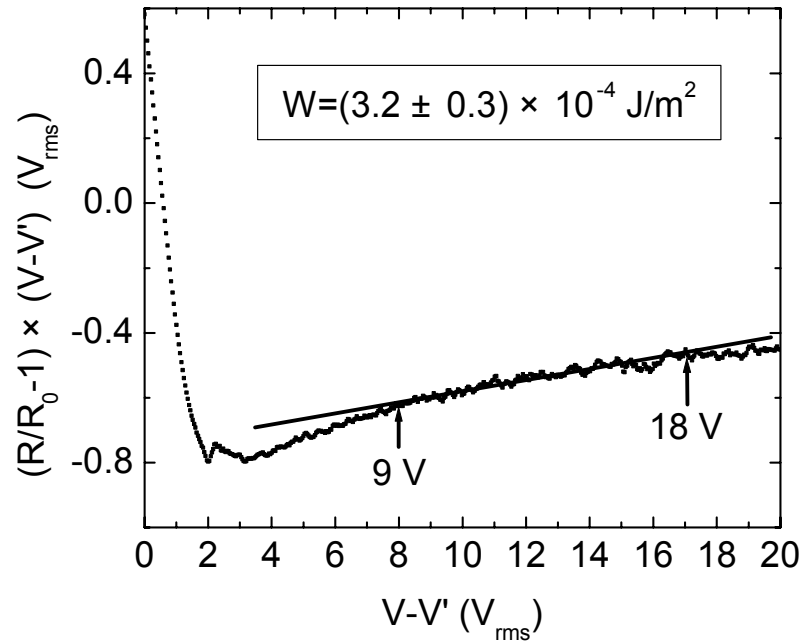


Figure 3.7: Illustration of the slope fitting method according to Eq.(3.10). A Linear fitting and a measurement result of  $W=(3.2\pm 0.3)\times 10^{-4}\ \text{J/m}^2$  are obtained for the  $7\ \mu\text{m}$  MLC-6608 VA cell. The LC cell capacitance measurement is avoided by adopting Eq.(3.8).

### **3.5 Discussion**

Various techniques for measuring the polar anchoring energy have been developed and many experimental results of different LC materials and substrates have been reported previously. However, reproducibility is a serious concern. Several research groups have derived different results even with similar or the same LC materials and substrates. This is due to the intrinsic complexity of anchoring interaction between LC materials and substrates surfaces. [49]

For accurate measurement of anchoring energy, the experimental setup, cells, and LC materials all require careful preparations. Light leakage from experimental setup needs to be minimized. Environment temperature may also greatly influence the results, since anchoring energy increases with decreasing temperature [50]. In addition, the accuracy of anchoring energy measurement depends on the LC layer thickness. The measured result from a thicker cell is usually smaller than that from a thin cell. This effect has been discussed in Ref.51 and a possible reason is ionic effect. With electric field, ions in the LC cells are adsorbed at opposite interfaces which cause additional space charge field. This field may influence the LC directors' reorientation. Such an ion-induced space charge field is difficult to calculate accurately. The overall effect is that a smaller anchoring energy is obtained for a thicker LC cell. This observation is consistent for both homogeneous and VA cells.

Thick cells are usually desired for electric field techniques. In our proposed VA anchoring energy measurement technique, thick cells may lead to a large  $V_{\max}$  and wide voltage range between  $V_{\min}$  and  $V_{\max}$ . If the anchoring is too weak and the cell is not thick

enough, the curve in the  $V > V_{\min}$  region tends to be nonlinear. The reason is that  $\Delta\theta$  is large and the assumption  $\sin(\Delta\theta) \approx \Delta\theta$  is no longer valid. In this case, a linear fitting over  $V_{\min}$  can not be obtained. In most experiments, the PI alignment film is  $\sim 60-80$  nm which is much thinner than the LC cell gap (a few microns). Thus, its contribution to the experimental results is very negligible.

The in-plane inhomogeneity of LC alignment may also contribute to the error of the experimental measurements. In theory, the VA LC directors are all in x-z plane, that is,  $n(y)=0$ . However, if a VA cell is not aligned well, then  $n(y)$  may not be close to zero. In the voltage-on state, the LC directors on the substrates will not be reoriented only in the x-z plane. Under this condition, the transmission of the VA LC cell does not follow the description of Eq.(4.11). Serious in-plane inhomogeneous alignment of VA cells may result in a large discrepancy in measurement. The quality of VA alignment can be checked by running the transmittance between crossed and parallel polarizers. Between crossed polarizers, the VA cell should exhibit a very high contrast ratio at normal incidence. In a voltage-on state, a good VA cell should also exhibit a good dark state at a given voltage and a laser wavelength under the parallel polarizer/analyzer configuration.

# CHAPTER FOUR: ANCHORING ENERGY AND CELL GAP EFFECTS ON LIQUID CRYSTAL RESPONSE TIME

## 4.1 Introduction

Response time of liquid crystal (LC) plays a crucial role for LC devices. The conventional understanding is that LC response (decay) time  $\tau_0$  is proportional to  $d^2$ , where  $d$  is the cell gap [52]. Here, the underlining assumption is the anchoring energy on LC-substrate surfaces is strong ( $W \rightarrow \infty$ ). However, some LC devices have relatively weak anchoring energy, such as LC cells with multi-domain vertical alignment (MVA) or with photoalignment. As a result, the  $\tau_0 \sim d^2$  dependence no longer holds. Therefore, it is essential to study the anchoring energy and cell gap effects on LC response time.

In this Chapter, we use two different approaches: effective cell gap and surface dynamic equation methods, to derive general analytical expressions of LC response time under finite anchoring energy conditions. The results of these two different approaches are consistent. We find the exponent  $x$  in  $\tau_0 \sim d^x$  depends on the anchoring energy  $W$  of the LC cell. Under strong and weak anchoring limits, the exponent  $x$  approaches 2 and 1, respectively.

In this Chapter, the derived analytical expressions correlates LC response time  $\tau_0$  with anchoring energy  $W$ , then  $W$  can be estimated from LC decay time. Up-to-date, a few experimental methods have been developed for characterizing the anchoring energy of LC cells [42, 43, 53]. Most of them are based on anchoring energy effect on LC cell's phase retardation in the high voltage region or its effect on the Freedericksz transition. The

method proposed in this Chapter provides another approach to study LC alignment techniques.

## 4.2. Theory

### 4.2.1 Effective Cell Gap Method

In this study, we choose a vertically-aligned (VA) LC cell as an example for analysis because it exhibits an unprecedented contrast ratio ( $>2000:1$ ) and more than 50% of LCD TVs use VA mode. These results and discussions are also valid to other LC modes. Figure 4.1 shows a VA nematic LC cell sandwiched between two parallel substrates and  $z = -d/2$  and  $d/2$  represent the bottom and top substrates, respectively. The  $z$ -axis is normal to the plane of the substrates and the electric field  $E$  is along the  $z$ -axis.

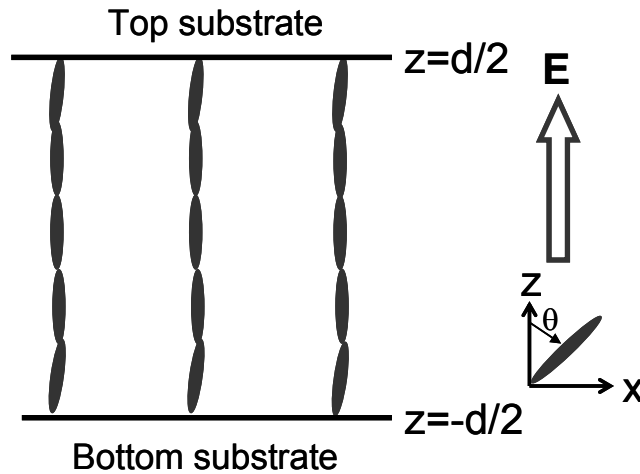


Figure 4.1: Schematic drawing of a VA LC cell.

Under such a device configuration, the LC dynamics can be described by the Erickson-Leslie equation. When the backflow and inertial effects are ignored [54, 55] the Erickson-Leslie equation has the following simplified expression:

$$\left(K_{11} \sin^2 \theta + K_{33} \cos^2 \theta\right) \frac{\partial^2 \theta}{\partial Z^2} + (K_{33} - K_{11}) \sin \theta \cos \theta \left(\frac{\partial \theta}{\partial Z}\right)^2 + \varepsilon_o \Delta \varepsilon E^2 \sin \theta \cos \theta = -\gamma_1 \frac{\partial \theta}{\partial t}, \quad (4.1)$$

where  $\gamma_1$  is the rotational viscosity,  $K_{11}$  and  $K_{33}$  represent the splay and bend elastic constants, respectively,  $\varepsilon_o \Delta \varepsilon E^2$  is the electric field energy density,  $\Delta \varepsilon$  is the LC dielectric anisotropy, and  $\theta$  is the tilt angle defined as the angle between z-axis and LC directors. In general, Eq.(4.1) can only be solved numerically. However, when the tilt angle is small ( $\sin \theta \sim \theta$ ) (small angle approximation) [19] and  $K_{33} \sim K_{11}$  (single elastic constant approximation), the Erickson-Leslie equation is reduced to:

$$K_{33} \frac{d^2 \theta}{dz^2} + \varepsilon_o \Delta \varepsilon E^2 \theta = -\gamma_1 \frac{\partial \theta}{\partial t}. \quad (4.2)$$

Under strong anchoring ( $W \rightarrow \infty$ ) condition, the LC directors on the substrates are fixed on their easy axis. Here, easy axis stands for the directions of LC directors which minimize the energy of the surface regions [56]. In some high contrast display devices, the pretilt angle is zero. Under such condition, the following boundary conditions hold

$$\theta_{z=-\frac{d}{2}, \frac{d}{2}} = 0. \quad (4.3)$$

Under the above boundary conditions, when the applied voltage exceeds the Freedericksz transition threshold, the LC directors are reoriented by the electric field. At a given voltage, the tilt angle can be expressed as following:

$$\theta = [\theta_s \sin(\beta z) + \theta_m \cos(\beta z)] \exp(-t / \tau). \quad (4.4)$$

In Eq.(4.4),  $\theta_m$  is the maximum tilt angle which occurs in the center of the LC cell ( $\theta|_{z=0} = \theta_m$ ), and  $\theta_s$  is found to be 0 when the pretilt angle is symmetric on the top and bottom substrates. Under these conditions, analytical solutions for rise time ( $\tau_r$ ) and decay time ( $\tau_d$ ) exist:

$$\tau_d = \tau_o = \frac{\gamma_1 d^2}{K_{33} \pi^2}, \quad (4.5)$$

$$\tau_r = \frac{\gamma_1}{\left| \varepsilon_0 |\Delta\varepsilon| E^2 - \frac{\pi^2}{d^2} K_{33} \right|} = \frac{\tau_o}{\left| \left( \frac{V}{V_{th}} \right)^2 - 1 \right|}. \quad (4.6)$$

In Eq.(4.6), the threshold voltage  $V_{th}$  is related to the bend elastic constant and dielectric anisotropy as:

$$V_{th} = \pi \sqrt{\frac{K_{33}}{\varepsilon_0 |\Delta\varepsilon|}}. \quad (4.7)$$

However, when the anchoring energy of the LC cell is not strong, the simple boundary conditions described in Eq.(4.3) no longer hold, and the validity of Eqs.(4.5) and (4.6) is in doubt. When the anchoring energy  $W$  is finite, we use the extrapolation length concept [57] to derive the analytical solutions for the LC response time.

As shown in Figure 4.2, the parameter  $b = K / W$  has the dimension of length, which is usually called *extrapolation length* and  $W$  is the polar anchoring energy strength coefficient, also called *anchoring energy*. For a VA cell, the azimuthal anchoring is not involved and  $K = K_{33}$ , the bend elastic constant.

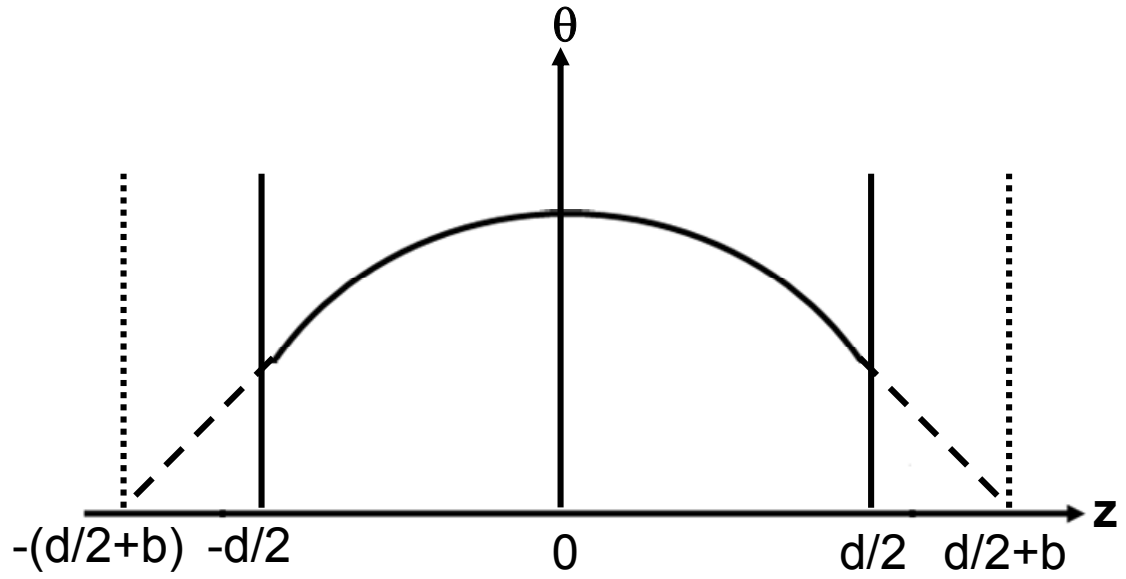


Figure 4.2: The  $z$ -coordinate dependent tilt angle  $\theta$ . The LC cell's physical surfaces are at  $z = \pm \frac{d}{2}$ . The  $\theta$  profile is extrapolated to  $z = \pm(\frac{d}{2} + b)$ , where  $\theta=0$ .  $b=K/W$  is the extrapolation length.

The extrapolation length  $b$  can be interpreted as the extension of the LC cell gap [58]. For example, an infinity anchoring ( $W \rightarrow \infty$ ) means no extension since  $b=0$ . On the other hand, weak anchoring implies to a large  $b$ , i.e., a large extension of the LC cell gap. For an LC cell with a finite anchoring energy, the LC directors on the physical substrate boundaries ( $z = \pm \frac{d}{2}$ ) will still be reoriented by the external electric fields. According to the definition of extrapolation length,  $\theta$  is zero at  $z = \pm(\frac{d}{2} + b)$ . Therefore,  $z = \pm(\frac{d}{2} + b)$  can be considered as virtual boundaries of the LC cell and the effective cell gap becomes

$$d' = d + 2b. \quad (4.8)$$

Here we consider the top and bottom substrates having the same alignment conditions. If the two substrates' alignments are different, then the effective cell gap is  $d' = d + b_b + b_t$ , where  $b_b$  and  $b_t$  represent the extrapolation length of the bottom and top substrates, respectively.

Based on this effective cell gap concept, we can modify Eqs.(4.5) and (4.6) to further derive the LC response time when  $W$  is finite. Both decay time  $\tau'_o$  and rise time  $\tau'_r$  can be derived if we replace the physical cell gap  $d$  with the effective cell gap  $d'$ :

$$\tau'_o = \frac{\gamma_1 d'^2}{K\pi^2} = \frac{\gamma_1}{K\pi^2} (d + 2b)^2 = \frac{\gamma_1}{K\pi^2} \left( d^2 + \frac{4dK}{W} + \frac{4K^2}{W^2} \right). \quad (4.9)$$

From Eq.(4.9), if  $2b \ll d$ , then the anchoring effect is negligible and  $d' \approx d$ . Under the strong anchoring limit, Eq.(4.9) is reduced to Eq.(4.5). For an intermediate anchoring strength,  $2K/W$  is not completely negligible. Therefore, we have to consider the anchoring energy terms shown in the right hand of Eq.(4.9). Because the quadratic term  $[(K/W)^2]$  in Eq.(4.9) is independent of cell gap and its magnitude is small as will be shown later, for the interest of understanding cell gap effect, we only consider the first two terms. Under this condition, Eq. (4.9), reads as

$$\tau'_o \approx \frac{\gamma_1}{K\pi^2} \left( d^2 + \frac{4dK}{W} \right). \quad (4.10)$$

This equation suggests that  $\tau'_o \sim d^2$  is accurate if  $d \gg 4K/W$ , i.e., strong anchoring energy. But when  $W$  is small, the first order term  $4dK/W$  has to be considered and  $\tau'_o \sim d^2$  is no longer accurate. Under a very weak anchoring condition where  $4K/W \gg d$ , the LC directors response time is reduced to

$$\tau_o' \approx \frac{4\gamma_1 d}{W\pi^2}. \quad (4.11)$$

Equation (4.10) suggests that the exponent  $x$  in  $\tau_o' = d^x$  lies between 1 and 2, where  $x \sim 1$  if the anchoring energy is very weak, while  $x \sim 2$  if the anchoring energy is very strong.

Similar correlations hold for rise time  $\tau_r'$  as well, i.e., by replacing  $d$  with  $d'$  in Eq.(4.6). Please note that threshold voltage  $V_{th}$  is also dependent on the anchoring energy. Thus, Eq.(4.7) needs to be modified when  $W$  has a finite value. As a result, Eq.(4.6) would have a much more complicated expression.

### 4.2.2 Surface Dynamic Equation Method

Another approach to study anchoring energy effect is to use the surface dynamic equation method [51]. If anchoring energy is finite, the simple boundary condition described in Eq.(4.3) is no longer valid. Instead, surface dynamic equation can be used to represent LC directors' reorientation on the LC-substrate boundaries:

$$\left(K_{11} \sin^2 \theta + K_{33} \cos^2 \theta\right) \frac{\partial \theta}{\partial Z} \pm \frac{df_s}{d\theta} = \gamma_s \frac{\partial \theta}{\partial t}, \quad (4.12)$$

where,  $f_s = \frac{1}{2}W \sin^2 \theta$  stands for the anchoring energy density on the boundaries, and  $\gamma_s$  is the surface rotational viscosity, and “+” and “−” signs are taken at  $z=d/2$  and  $z=-d/2$ , respectively. Analytical expressions can be derived following the approach reported in Ref.[51]. Because the characteristic time of the surface LC director reorientation is much longer than that of the corresponding LC directors in the bulk, the surface term  $\gamma_s \partial \theta / \partial t$  in Eq.(4.12) can be ignored. Under small angle approximation, Eq.(4.12) is simplified to:

$$K_{33} \frac{\partial \theta}{\partial Z} \pm W \theta = 0. \quad (4.13)$$

By solving Eqs. (4.4) and (4.13), we derive the following decay time and rise time:

$$\tau'_d = \tau'_o = \frac{\gamma_1}{\beta^2 K_{33}}, \quad (4.14)$$

$$\tau'_r = \frac{\gamma_1}{\left| \varepsilon_o |\Delta \varepsilon| E^2 - \beta^2 K_{33} \right|}, \quad (4.15)$$

where  $\beta$  satisfies the following equation:

$$tg(\beta d) = \frac{2W / K_{33} \beta}{1 - (W / K_{33} \beta)^2}. \quad (4.16)$$

If  $W \rightarrow \infty$  (strong anchoring), the right term of Eq.(4.16) approaches 0 from negative side. Thus, we find  $\beta = \pi/d$ . Under this condition, Eqs.(4.14) and (4.15) are reduced to Eqs.(4.5) and (4.6).

If  $W \rightarrow 0$ ,  $tg(\beta d)$  is small and it can be approximated by  $\beta d$ . Solving Eq.(4.16) we obtain:

$$\beta^2 \approx \frac{\left( \frac{Wd}{K_{33}} + 2 \right) W}{K_{33} d}. \quad (4.17)$$

When  $Wd/K_{33} \ll 1$ , Eq. (4.17) can be approximated as  $\beta^2 \approx 2W / (K_{33} d)$ . Under such a circumstance, the decay time and rise time have following expressions:

$$\tau'_d = \tau'_o \approx \frac{\gamma_1 d}{2W}, \quad (4.18)$$

$$\tau'_r = \frac{\gamma_1}{\left| \varepsilon_o |\Delta \varepsilon| E^2 - 2W / d \right|}. \quad (4.19)$$

Eq.(4.18) also leads to  $\tau'_o \sim d$  for the case of weak anchoring energy, which is consistent with the result we derived using the effective cell gap method. The only difference is their coefficients. In Eq.(4.13), the coefficient is  $(2/\pi)^2$  which is  $\sim 0.41$ , while in Eq.(4.18) the coefficient is 0.5. This 20% difference arises from the approximations during the derivation processes of Eqs.(4.13) and (4.18).

### 4.2.3 Results and Discussion

For an LC device, the total response time is usually referred to the sum of rise and decay times. The rise time is strongly dependent on the applied voltage, as shown in Eq.(4.6). When the applied voltage is only slightly above  $V_{th}$ , the rise time is slow. To overcome the slow rise time, an overdrive voltage technique [59] has been commonly practiced in LCD industry. Therefore, here we focus our discussion on the LC decay process.

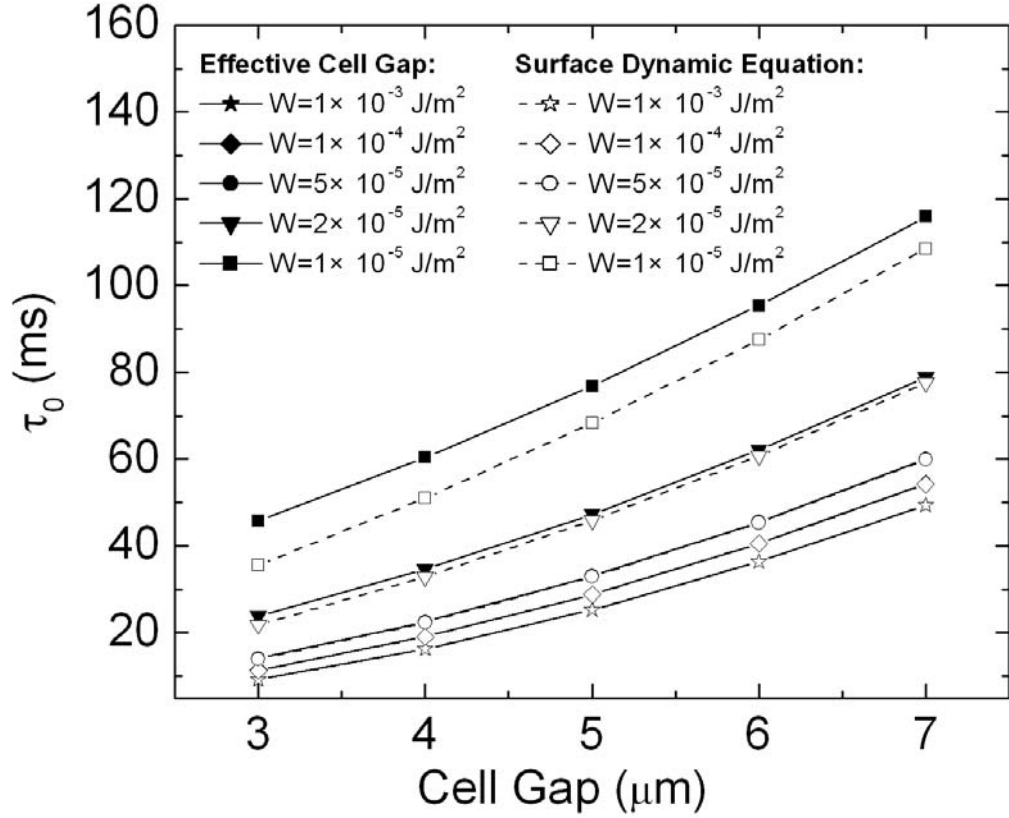


Figure 4.3: Anchoring energy ( $W$ ) and cell gap ( $d$ ) dependent LC decay time ( $\tau'_d = \tau'_o$ ). The solid lines represent the results of the effective cell gap method, and the dashed lines are based on the surface dynamic equation method. When  $W$  is large, the results of these two methods are almost identical as the bottom three curves ( $W=1 \times 10^{-3}$ ,  $1 \times 10^{-4}$  and  $5 \times 10^{-5}$  J/m<sup>2</sup>) show.

Figure 4.3 shows the simulated cell gap dependent LC decay time under various anchoring strengths. The LC mixture used for calculations is Merck MLC-6608 whose physical properties (at 20°C) are listed as follows:  $K_{11}=16.7$  pN,  $K_{33}=18.1$  pN,  $\epsilon_{//}=3.6$ ,  $\epsilon_{\perp}=7.8$ ,  $\gamma_l=0.186$  Pas,  $n_o=1.475$ , and  $n_e=1.558$ . Five cell gaps were studied:  $d=3, 4, 5, 6$ , and  $7$  μm. As the cell gap increases, the first transmission maximum occurs at a lower voltage,

but the threshold voltage remains the same. In each cell, the assumption of small angle approximation is still valid.

Table 4.1: Anchoring energy  $W$  dependent  $x$  value, where  $x$  is the exponent of  $\tau_o \sim d^x$ . The data are obtained from the fitting of solid lines in Figure 4.3.

<b>W (J/m<sup>2</sup>)</b>	$1 \times 10^{-3}$	$1 \times 10^{-4}$	$5 \times 10^{-5}$	$2 \times 10^{-5}$	$1 \times 10^{-5}$
<b><math>x</math></b>	1.98	1.84	1.71	1.41	1.09

During simulations, we calculate the LC directors decay time from the first transmission maximum to  $V=0$ . We then use the extrapolation length method (solid lines) and surface dynamic equation method (dashed lines) to fit the simulated data using  $\tau_o \sim d^x$ . Table 4.1 lists the obtained  $x$  values from the solid lines fittings. From Table 4.1, we find that  $x \approx 2$  is valid only when the anchoring is strong ( $W \sim 1 \times 10^{-3}$  J/m<sup>2</sup>). As the anchoring energy gets weaker, the exponent gets closer to 1. These results confirm that the conventional understanding of  $\tau_o \sim d^2$  is only valid when  $W \rightarrow \infty$ , and the quadratic dependence is no longer accurate if the LC cells have a finite anchoring energy.

In Figure 4.3, the effective cell gap and surface dynamic equation methods lead to consistent results when the anchoring energy is larger than  $1 \times 10^{-4}$  J/m<sup>2</sup>. However, an appreciable amount of discrepancy ( $\sim 30\%$ ) is observed when the anchoring energy is low ( $W = 1 \times 10^{-5}$  J/m<sup>2</sup>). We will discuss its causes later. The surface dynamic equation method is

relatively complicated, since a simple analytical solution of Eq.(4.16) is not available. Therefore, we have to solve Eq.(4.16) numerically. This is especially difficult when  $\beta d \sim \pi/2$  in Eq.(4.16). If the alignment conditions are different on the bottom and top substrates, then the surface dynamic equation method would be even more complicated. Since these two methods show similar results in the major cases shown in Figure 4.3, the effective cell gap method is easier and more practical.

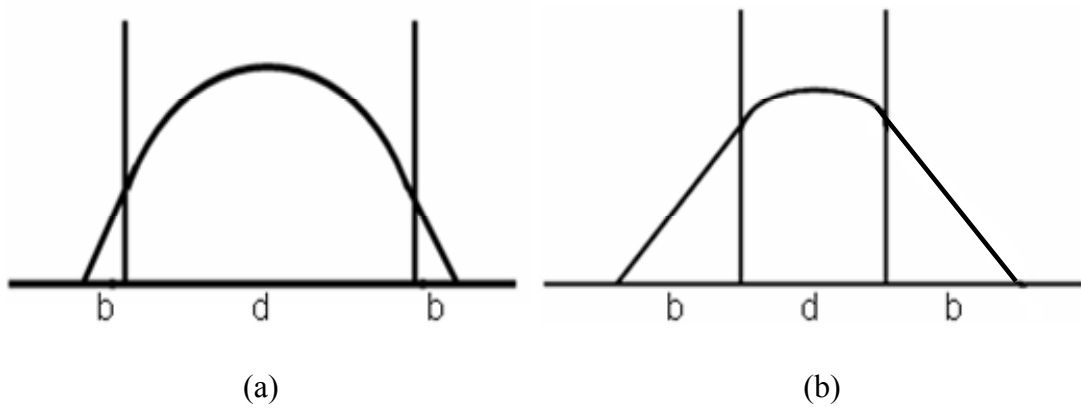


Figure 4.4: (a) When  $d \gg b$ , the extrapolation length approximation is accurate; (b) When  $d \sim b$ , the approximation is less accurate.

To further analyze the accuracy of the effective cell gap method, two different extrapolation length conditions are plotted in Figure 4.4. In Figure 4.4(a),  $d \gg b$  and the extrapolation length method is pretty accurate. But when the cell gap is relatively small and the anchoring energy is weak as Figure 4.4(b) shows, the extrapolation length method would be less accurate. In Figure 4.3, if we compare the two curves for  $W = 1 \times 10^{-5} \text{ J/m}^2$ , the

difference between the solid and dashed lines is attributed by this approximation. When  $W=1\times 10^{-5}$  J/m<sup>2</sup>, the  $b$  ( $=K/W$ ) value is as large as 1.81  $\mu\text{m}$ . Thus, the linear extrapolation of the LC cell gap would not be accurate for thin cells. For instance, if  $d=3$   $\mu\text{m}$  the difference between these two methods is 28.7%. But for a 7  $\mu\text{m}$  LC cell, the difference is reduced to 7.4%.

### **4.3 Experiment**

Based on Eq.(4.9), we can estimate anchoring energy  $W$  by measuring the LC decay time. Since LC decay time is related to the LC material's properties ( $\gamma_1$ ,  $K$ ), cell gap  $d$ , and anchoring energy  $W$ , we can calculate  $W$  by measuring  $\tau_o$ , provided that  $\gamma_1$ ,  $K$  and  $d$  are known. From Figure 4.3, we find that the LC decay time is especially sensitive to anchoring energy when the anchoring energy is in the intermediate to weak range. Therefore, this method is applicable to LC cells with a relatively weak anchoring energy.

Two types of VA cells have been used for display applications: strong rubbing and rubbing-free [4]. The rubbed or sputtered cells tend to have strong anchoring energy and the rubbing-free cells tend to have a weak anchoring energy. In the former case, such as liquid-crystal-on-silicon(LCOS) for projection displays, a uniform pretilt angle ( $\sim 2\text{-}3^\circ$ ) is generated by sputtered inorganic SiO<sub>2</sub> layers [60]. In the wide-view LCD TVs, patterned vertical alignment (PVA) [61] and multi-domain vertical alignment (MVA) [62] cells are the two common choices. In these cells, both top and bottom substrates are coated with a thin polyimide layer, but without rubbing. In a PVA cell, there is no pretilt angle; the LC

directors' reorientation direction is controlled by the fringing fields. In a MVA cell, a small pretilt angle exists only near the protrusions.

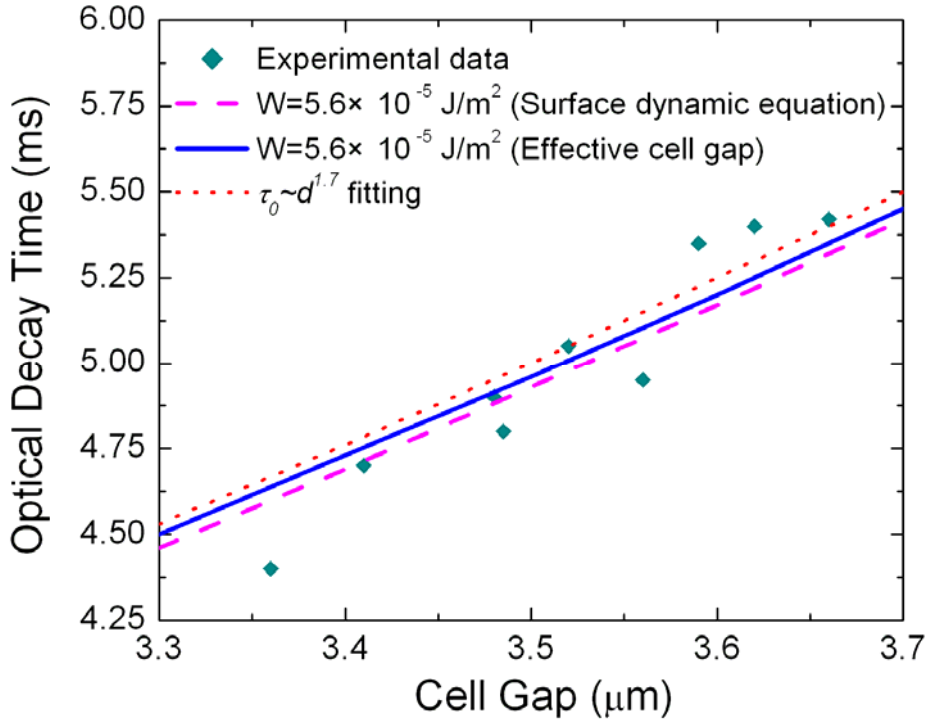


Figure 4.5: Experimental results of the cell gap dependent LC optical decay time. Stars are the measurement data. The solid line is the fitting curve using the effective cell gap method Eq. (4.9), and the pink dashed line is based on the surface dynamic equation method. From fittings, the anchoring energy is found to be  $W=5.6 \times 10^{-5} \text{ J/m}^2$ . The red dotted lines represent the fitting curve using  $\tau_0 \sim d^{1.7}$ .

In our experiment, we used MVA cells with various cell gaps. The cell gap was measured by counting the Fabry-Perot interference fringes from a spectrophotometer. The cells were filled with a commercial LC mixture, MLC-6608. We first measured the voltage-dependent

transmittance between crossed polarizers and then measured the optical decay time. All the measurements were performed using a He-Ne laser beam. Its wavelength is  $\lambda=633$  nm.

Figure 4.5 shows the measured LC optical decay time (90-10%) [60] of several MVA cells. The experimental data (dots) were collected at 38.5° C, which is the LCD-TV's operating temperature after fully warm-up. We then fit the data using three models: solid line stands for the effective cell gap model [Eq.(4.9)], with  $W=5.6 \times 10^{-5}$  J/m<sup>2</sup>, dashed lines for the surface dynamic equation [Eq.(4.16)] with  $W=5.6 \times 10^{-5}$  J/m<sup>2</sup>, and dotted lines for the simplified equation  $\tau_o \sim d^x$  with  $x=1.7$ . These three curves all fit the experimental data well. When  $W=5.6 \times 10^{-5}$  J/m<sup>2</sup>, the extrapolation length of these cells is calculated to be  $b=0.34$   $\mu\text{m}$ . For example, if an LC cell has 3.5  $\mu\text{m}$  cell gap, then the  $d^2$ ,  $4dK/W$  and  $4K^2/W^2$  terms in Eq.(4.9), contribute 70.3%, 26.1% and 2.6% to  $\tau'_o$ , respectively. This confirms that in Eq.(4.9), the  $4dK/W$  term needs to be considered, but the  $4K^2/W^2$  term is negligible.

It is known that LC material and cell gap significantly influence LC device's response time, but the anchoring effect is not well studied quantitatively previously. From Eqs.(4.11) and (4.18), anchoring energy plays an important role to affect the LC response time. Within the weak anchoring regime, the LC decay time is inversely proportional to the anchoring energy. For instance, if we can find a polyimide that has a somewhat larger anchoring with the LC material, then the decay time can be improved.

#### **4.4 Discussion of Thin Cell Gap Effect**

As mentioned in Chapter Two, response time of liquid crystal devices can be improved by reducing cell gap and using high birefringence LC material. Recently, LC cells with very thin cell gap ( $\sim 1 \mu\text{m}$ ) have been demonstrated for fast response time purpose [63]. The LC cells used in some LCOS projection displays are even thinner ( $\sim 0.8 \mu\text{m}$ ), as reflective displays only need relative thin cell gap to realize  $\pi$  phase retardation.

LC response time is especially critical for the promising color sequential LCD. In color sequential LCD, red, green and blue (RGB) sub-frames are displayed sequentially, and each sub-frame shows only the distribution of a primary color (red, green or blue) of a full-color image. If the sub-frames are displayed at a fast frame rate, usually three-times of the video rate (180 Hz), the human eyes can integrate these RGB sub-frames temporally, yielding a perceived full-color image. In this case, every pixel displays RGB colors at different time and there is no spatial division of RGB pixels. With RGB-LED backlight, color filters are not needed in color sequential LCDs, which significantly improves the power efficiency of LCD devices ( $\sim 3X$ ). However, for the color sequential LCDs, very fast LC response time is essential and LC cells with thin cell gap are one of the solutions.

When LC cell gap is reduced, the anchoring energy effects become even more important, because the two boundary regions occupy more of the LC cell and the bulk region occupies less. For example, the extrapolation length  $b \sim 0.34 \mu\text{m}$  in our experiments, and  $2b$  is already very close to the thin cell gap ( $\sim 1 \mu\text{m}$ ); therefore its effect must be considered in the response time simulation.

Using FEM numerical simulation program, the anchoring energy effects on thin LC cells' response time is studied. The surface dynamic equation Eq.(4.12) is used as the boundary conditions in the numerical simulation program. The simulation parameters are: surface viscosity  $\gamma_s=3\times 10^{-6}$  Ns/m,  $K_{11}=16.7$  pN,  $K_{22}=7.0$  pN,  $K_{33}=18.1$  pN and  $\Delta\varepsilon=5.7$ . According to the LC cell gap, the birefringence  $\Delta n$  is adjusted to make the phase retardation  $\delta=\pi$ , which is necessary for display applications. Two anchoring energy conditions are simulated, one is the ideal case of  $W\sim\infty$  and the other is  $W=1\times 10^{-4}$  J/m<sup>2</sup>, which is usually considered to be relatively strong anchoring.

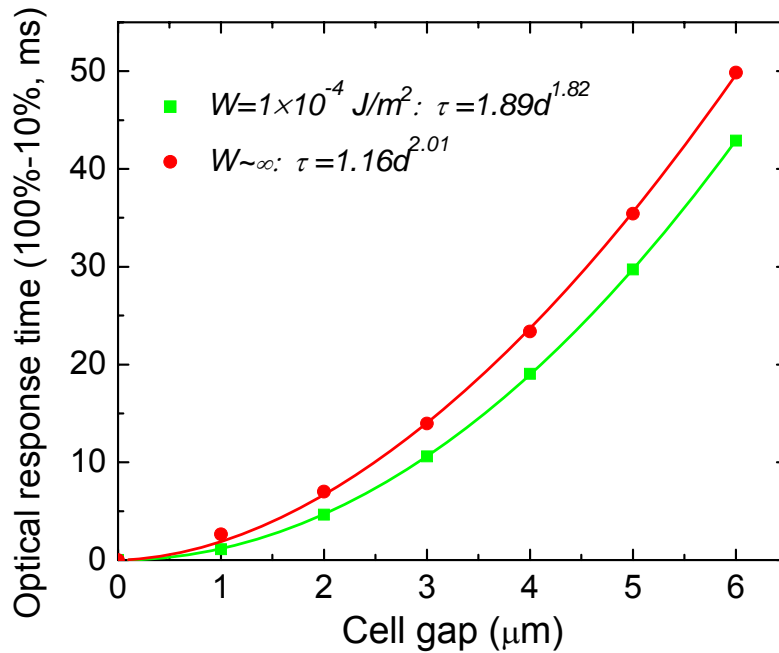


Figure 4.6: Numerical simulation results of cell gap and anchoring energy dependent LC response time(100%-10%). The cell gap  $d$  is between 0 ~6.0  $\mu\text{m}$ , and the anchoring energy  $W=1\times 10^{-4}$  J/m<sup>2</sup> and  $\sim\infty$ .

Figure 4.6 shows the numerical simulation results of cell gap and anchoring energy dependent LC response time (100%-10%). When  $W=1\times 10^{-4} \text{ J/m}^2$ , the response time is larger than that of  $W\sim\infty$ . For example, when  $d\sim 6 \mu\text{m}$ , the response time of  $W=1\times 10^{-4} \text{ J/m}^2$  is about 16% larger than that of  $W\sim\infty$ . But when the cell gap becomes smaller, the difference gets more significant. It is 51.2% if  $d=2 \mu\text{m}$  and 142% when  $d=1 \mu\text{m}$ . These results confirm our previous theoretical analysis that the anchoring energy effect is more important if LC cell is thinner. We use the  $\tau_{optical}\sim d^x$  correlation to fit the simulation results in Figure 4.6, and  $\tau_{optical}$  is the optical response time(100%-10%). When  $W=1\times 10^{-4} \text{ J/m}^2$ ,  $x=1.82$ , and  $x=2.01$  if  $W\sim\infty$ . These results perfectly match our results in Table 4.1 and also the previous theory.

To further study the thin cell gap effect, we plot the simulation results of thin cell gap(0.4  $\mu\text{m}\sim 1.0 \mu\text{m}$ ) dependent LC response time(100%-10%) in Figure 4.7. When cell gap  $d=0.4 \mu\text{m}$ , the LC response time of  $W=1\times 10^{-4} \text{ J/m}^2$  is about 4 times faster than that of  $W\sim\infty$ . This significant difference must be considered for ultra-thin LC cells. We use  $\tau_{optical}\sim d^x$  to fit the numerical simulation results, and the results are,  $x=1.33$  when  $W=1\times 10^{-4} \text{ J/m}^2$ , and  $x=2.13$  if  $W\sim\infty$ . For the  $W=1\times 10^{-4} \text{ J/m}^2$  case, the ratio between extrapolation length and cell gap,  $b/d$ , gets larger if  $d$  is smaller, so the first order term in Eq.(4.9) must be considered and it significantly influences the LC response time.

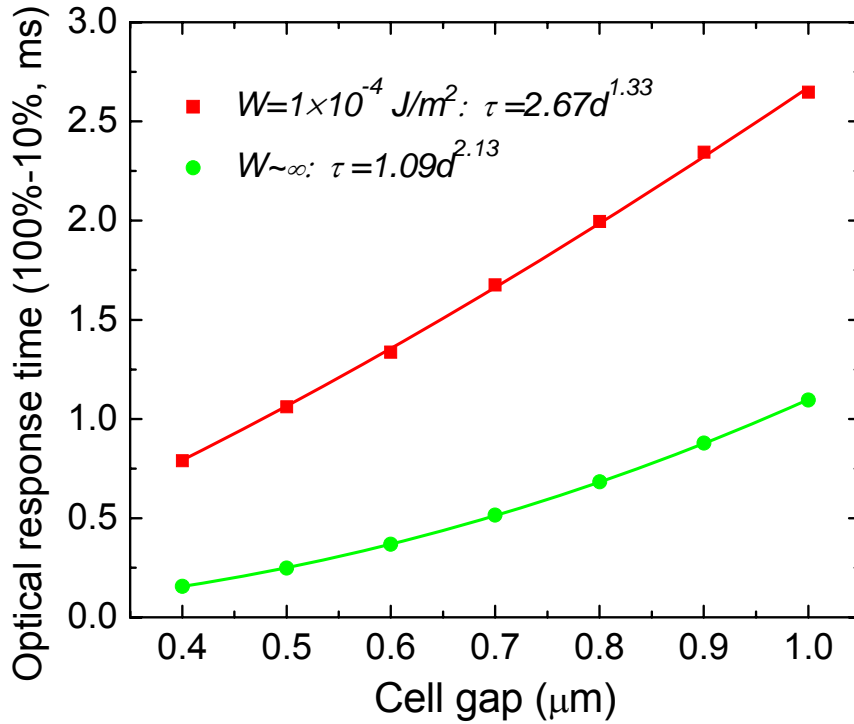


Figure 4.7: Numerical simulation results of thin cell gap (0.4~1  $\mu\text{m}$ ) and anchoring energy dependent LC response time(100%-10%). Two anchoring energy cases are simulated:  $W=1 \times 10^{-4} \text{ J/m}^2$  and  $W \sim \infty$ .

#### 4.5 Summary

We derived the analytical expressions for understanding the anchoring energy effect on the LC response time. Two different approaches: extrapolation length and surface dynamics are employed to study this effect. Both models fit with experimental data well. In addition, a simplified equation  $\tau_0 \sim d^x$  was used to fit the experimental data. Under strong and weak anchoring limits, the exponent is close to  $x \sim 2$  and  $x \sim 1$ , respectively. For the tested MVA

cells, the anchoring energy is finite and the exponent is found to be  $x \sim 1.7$ . By optimizing the LC and polyimide interactions, it is possible to optimize the LC response time.

The novel theoretical analysis is especially important for LC devices with thin cell gaps, because the anchoring energy effect becomes more important under this condition. Thin cell gap is a promising approach to realize fast LC response time. Therefore, this work may have important impact on future LCD designs.

# CHAPTER FIVE: PRETILT ANGLE EFFECTS ON LIQUID CRYSTAL RESPONSE TIME

## 5.1 Introduction

Liquid crystal response time plays a crucial role for display applications. A slow response time causes undesirable image blurring and should be avoided. LC response time is significantly influenced by the surface treatment of the substrates. A properly prepared substrate will orient the nematic LC directors in a preferred direction called pretilt angle [64]. Pretilt angle makes an important contribution to the dynamics of an LC cell [65]. However, detailed theoretical analysis has not been studied thoroughly.

In this chapter, we derive analytical expressions for describing the LC dynamics including the pretilt angle effect<sup>66</sup>. The analysis is valid for LC devices with pretilt angles, such as transfective displays with homogeneous alignment [67, 68] and LCoS displays with vertical alignment [60, 69, 70]. To confirm the theoretical analysis, we prepare several VA LC cells with various pretilt angles and measure their response times. In our experiments, we find that a large pretilt angle indeed greatly influences the LC response time. These experimental results are consistent with our theoretical analysis.

## 5.2 Theory

Figure 4.1 shows a vertically-aligned nematic LC layer sandwiched between two parallel substrates where  $z=-d/2$  and  $+d/2$  stand for the bottom and top substrates, respectively. The  $z$ -axis is normal to the plane of the substrates, and the electric field  $E$  is along the  $z$ -axis.

When the backflow and inertial effects are ignored, the Erickson-Leslie equation for describing the dynamics of LC directors is reduced to the following form [54, 55]:

$$\left(K_{11} \sin^2 \theta + K_{33} \cos^2 \theta\right) \frac{\partial^2 \theta}{\partial Z^2} + (K_{33} - K_{11}) \sin \theta \cos \theta \left(\frac{\partial \theta}{\partial Z}\right)^2 + \varepsilon_o \Delta \varepsilon E^2 \sin \theta \cos \theta = -\gamma_1 \frac{\partial \theta}{\partial t}. \quad (5.1)$$

In Eq.(5.1),  $\gamma_1$  is the LC rotational viscosity,  $K_{11}$  and  $K_{33}$  represent the splay and bend elastic constants, respectively,  $\varepsilon_o \Delta \varepsilon E^2$  is the electric field energy density,  $\Delta \varepsilon$  is the LC dielectric anisotropy, and  $\theta$  is the tilt angle defined as the angle between the z-axis and the LC directors.

In general, Eq.(5.1), can only be solved numerically. However, when the tilt angle is small ( $\sin \theta \sim \theta$ ) (small angle approximation) [19] and  $K_{33} \sim K_{11}$  (single elastic constant approximation), the Erickson-Leslie equation is simplified as:

$$K_{33} \frac{d^2 \theta}{dz^2} + \varepsilon_o \Delta \varepsilon E^2 \theta = -\gamma_1 \frac{\partial \theta}{\partial t}. \quad (5.2)$$

Eq.(5.2) has the following general solution:

$$\theta = [\theta_s \sin(\beta z) + \theta_m \cos(\beta z)] \cdot \exp(-t / \tau). \quad (5.3)$$

Let us assume the VA cells studied have the same top and bottom substrate alignment conditions. At a given voltage,  $\theta_m$  is the maximum tilt angle in the center of the LC cell ( $\theta|_{z=0} = \theta_m$ ), and  $\theta_s$  is found to be 0.

When the pretilt angle  $\theta_p$  is zero and the anchoring energy is strong, the following boundary conditions hold:

$$\theta_{Z=-\frac{d}{2}, \frac{d}{2}} = \theta_p = 0. \quad (5.4)$$

Equations (5.3) and (5.4) lead to the following well known analytical solutions for the decay ( $\tau_d$ ) and rise ( $\tau_r$ ) times:

$$\tau_d = \tau_o = \frac{\gamma_1 d^2}{K_{33} \pi^2}, \quad (5.5)$$

$$\tau_r = \frac{\gamma_1}{\left| \varepsilon_o |\Delta\varepsilon| E^2 - \frac{\pi^2}{d^2} K_{33} \right|} = \frac{\tau_o}{\left| \left( \frac{V}{V_{th}} \right)^2 - 1 \right|}. \quad (5.6)$$

In Eq.(5.5),  $\tau_o$  is called free relaxation time; i.e., during the decay process there is no bias voltage, and in Eq.(5.6), the threshold voltage is defined as:

$$V_{th} = \pi \sqrt{\frac{K_{33}}{\varepsilon_o |\Delta\varepsilon|}}. \quad (5.7)$$

If the pretilt angle departs from zero, then we have:

$$\theta_{z=-\frac{d}{2}, \frac{d}{2}} = \theta_p \neq 0, \quad (5.8)$$

Eq.(5.3) should satisfy the boundary conditions described by Eq.(5.8) at  $z = -\frac{d}{2}$  and  $\frac{d}{2}$ .

From Eqs. (5.3) and (5.8), we find the parameter  $\beta$  has following form:

$$\beta = \frac{2}{d} \cos^{-1} \left( \frac{\theta_p}{\theta_m} \right). \quad (5.9)$$

Based on Eq.(5.2), we derive the new response time that takes pretilt angle effect into consideration:

$$\tau_d^* = \tau_o^* = \frac{\gamma_1}{\beta^2 K_{33}}, \quad (5.10)$$

$$\tau_r^* = \frac{\gamma_1}{\left| \varepsilon_o |\Delta\varepsilon| E^2 - \beta^2 K_{33} \right|}. \quad (5.11)$$

In most cases, the maximum tilt angle is much larger than the pretilt angle, i.e.,  $\theta_m \gg \theta_p$ .

Under such a condition, the  $\cos^{-1}(\cdot)$  term in Eq.(5.9) can be approximated as:

$$\cos^{-1}\left(\frac{\theta_p}{\theta_m}\right) \sim \frac{\pi}{2} - \frac{\theta_p}{\theta_m}, \quad (5.12)$$

and we derive the response time as follows:

$$\tau_d^* = \tau_o^* = \frac{\gamma_1}{\beta^2 K_{33}} = \frac{\gamma_1 d^2}{4K_{33} \left(\frac{\pi}{2} - \frac{\theta_p}{\theta_m}\right)^2}, \quad (5.13)$$

$$\tau_r^* = \frac{\gamma_1}{\left| \varepsilon_o |\Delta\varepsilon| E^2 - \frac{4K_{33}}{d^2} \left(\frac{\pi}{2} - \frac{\theta_p}{\theta_m}\right)^2 \right|}. \quad (5.14)$$

Strictly speaking, the LC threshold voltage  $V_{th}$  no longer exists if the pretilt angle is nonzero, although the threshold-like behavior in the voltage-dependent transmittance still appears. For simplicity, let us assume the threshold voltage still exists. Under such a condition, Eq.(5.14) can be simplified as:

$$\tau_r^* = \frac{\tau_o^*}{\left| \left( \frac{V}{\left(1 - \frac{2\theta_p}{\pi\theta_m}\right)V_{th}} \right)^2 - 1 \right|}. \quad (5.15)$$

As expected, Eqs. (5.13) and (5.15) are reduced to Eqs.(5.5) and (5.6), when the pretilt angle is zero. Eqs.(5.13) and (5.15) suggest that the LC response time is also dependent on  $\theta_m$  which originates from the applied voltage. In [65], it is found that the pretilt angle effect

becomes more pronounced when  $V$  gets close to  $V_{th}$ . The derived expressions here confirm the bias voltage effect on LC response time, since  $\theta_m$  decreases when  $V$  gets smaller.

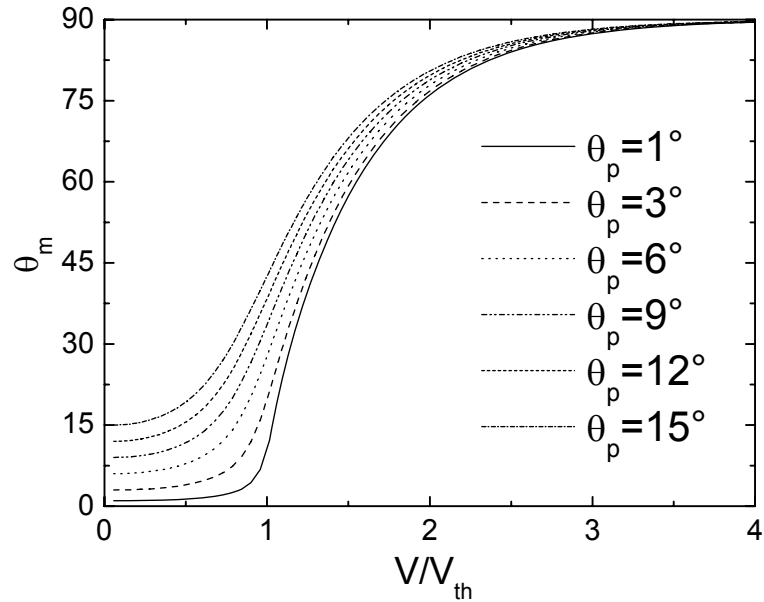


Figure 5.1: Voltage dependent  $\theta_m$ . The LC parameters used for simulations are:  $\Delta\epsilon=-4.2$ ,  $V_{th} = 2.19 V_{rms}$ ,  $K_{11}=16.7$  pN, and  $K_{33}=18.1$  pN.

Figure 5.1 shows the simulation results of the voltage dependent  $\theta_m$ . In the  $V_{th} < V < 4V_{th}$  region,  $\theta_m$  increases significantly when the applied voltage increases and eventually approaches  $90^\circ$  at  $V \sim 4V_{th}$ . Pretilt angles also influence  $\theta_m$ , especially when  $V$  is not too far above  $V_{th}$ .

For an LCD device, the total response time is usually referred to the sum of rise and decay times. The rise time is strongly dependent on the applied voltage, and is usually much smaller than the decay time. With overdriving technique [71], the rise time can be further

reduced. For this reason, the discussion in this paper will be focused on the LC decay process.

### **5.3 Experiment**

To confirm the theoretical analysis, we studied various VA LC cells which have different pretilt angles. For examples, two VA cells with the same rubbed polyimide were filled with two different negative LC materials. Both cells have strong anchoring energy ( $> 4 \times 10^{-4} \text{ J/m}^2$ ) [53] so that the anchoring energy effect on LC response time can be neglected. Their pretilt angles and decay times were measured at room temperature ( $T \sim 20^\circ\text{C}$ ) and  $\lambda = 633 \text{ nm}$ , respectively. It is known that pretilt angles are dependent on the LC materials even if the alignment conditions are the same [72, 73]. As a result, their pretilt angle effects on LC dynamics can still be different.

In experiments, the VA cells sandwiched between two crossed polarizers are biased at a voltage  $V_b$ , which corresponds to the first transmittance maximum. Under such a condition, the total phase change is  $\delta_0 = \pi$ . When the bias voltage is released instantaneously at  $t=0$ , the time-dependent transmittance can be converted to the transient phase decay described by  $\delta(t)$  [74]:

$$\delta(t) \approx \delta_0 \exp(-2t / \tau_o). \quad (5.16)$$

From Eq.(5.16),  $\tau_o$  can be experimentally extracted from linear fitting of the time dependent  $\ln(\delta_0/\delta(t))$  curve.

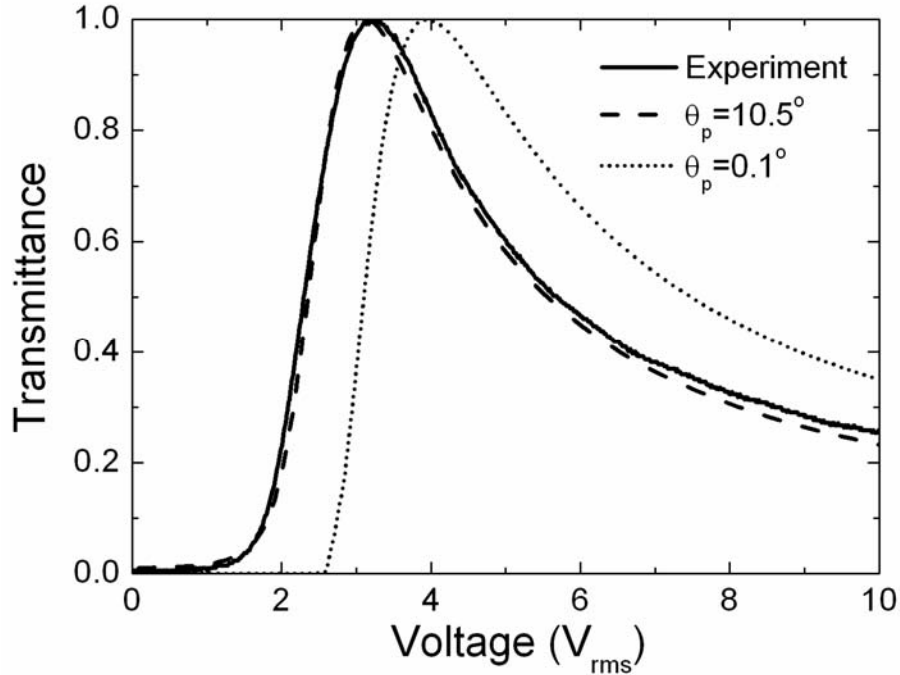


Figure 5.2: Voltage dependent transmittance curves of a 6.97  $\mu\text{m}$  VA cell at  $\lambda=633$  nm. The solid line is the experimental result, and dotted and dashed lines represent the simulation results for  $\theta_p=0.1^\circ$  and  $10.5^\circ$ , respectively.

In the first experiment, we filled a 6.97  $\mu\text{m}$  VA LC cell with a negative LC material A, which is a modified MLC-6608 mixture from Merck. By numerical fitting of the experimental data, the pretilt angle was found to be  $10.5^\circ$ . Figure 5.2 shows the voltage dependent normalized transmittance of the LC cell at  $\lambda=633$  nm and  $T\sim 20^\circ\text{C}$ . For comparison, numerically simulated curves under  $10.5^\circ$  and  $0.1^\circ$  pretilt angles are also plotted in the figure. A large pretilt angle smears the threshold behavior and lowers the effective threshold voltage. From Figure 5.2, the maximum transmittance occurs at  $V_b=3.25$   $V_{\text{rms}}$ , which corresponds to  $\delta_0=\pi$ . To measure decay time, we released the bias voltage and

recorded the voltage dependent transmittance by a LabVIEW system. The transmittance data were converted to transient phase change as plotted in Figure 5.3. A linear fitting of the experimental data leads to  $\tau_0 \sim 59 \pm 2.5$  ms. If the pretilt angle effect is not considered, then  $\tau_0$  is calculated to be 42 ms based on Eq.(5.5). The measured experimental result is  $\sim 40.5\%$  larger than the theoretical one. The discrepancy is rather significant. If we use the modified expression Eq.(5.13), the calculated result is  $\tau_0 \sim 52$  ms, which is  $\sim 11.3\%$  lower than the experimental data. In Eq.(5.13),  $\theta_m \sim 68^\circ$  is obtained from numerical simulation. By comparing the experimental and two theoretical results (including and excluding the pretilt angle effect), we find that the derived theoretical expression Eq.(5.13), describes the pretilt effect reasonably well. It indicates that the previously mentioned discrepancy mainly originates from the pretilt angle effect. Besides pretilt angle, backflow is another possible mechanism contributing to the discrepancy between the theoretical and experimental results. However, for a thin VA cell under low voltage operation the backflow effect should be relatively small.

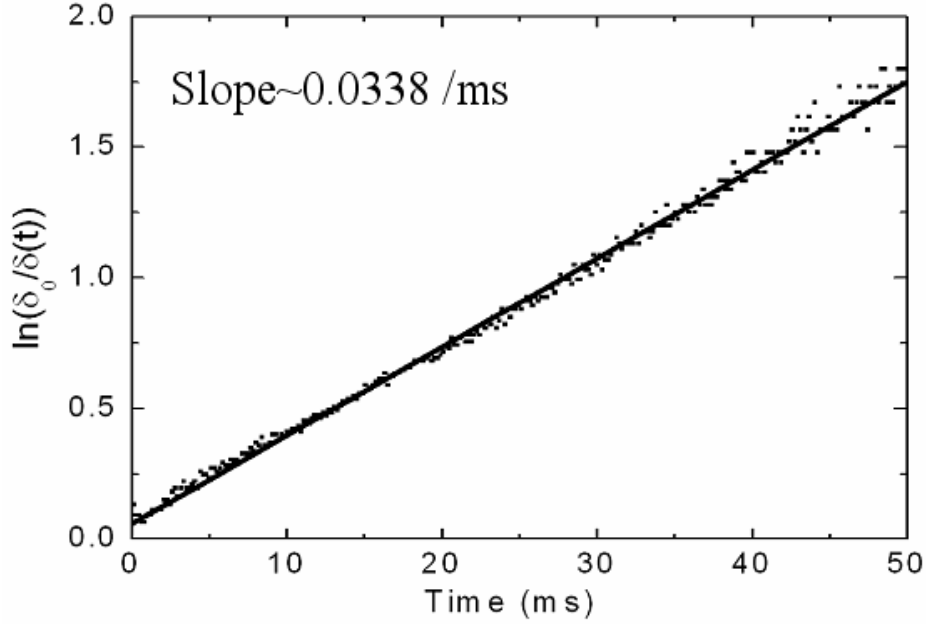


Figure 5.3: Time-dependent  $\ln[\delta_0/\delta(t)]$  of the 6.97  $\mu\text{m}$  VA cell. Dots are experimental data and solid line is the fitting curve. The slope of the straight line is 0.0338/ms, and  $\tau_0$  is found to be  $\sim 59$  ms.

In the second experiment, we tested a 7.10  $\mu\text{m}$  VA cell, which has the same surface treatment as the first sample. The cell was filled with a commercial negative LC mixture B (MCL-6608). At 20°C, the LC parameters for mixture B are:  $n_o=1.4748$ ,  $n_e=1.5578$  at  $\lambda=633$  nm,  $\Delta\epsilon=-4.2$ ,  $\gamma_1=186$  mPas,  $K_{11}=16.7$  pN, and  $K_{33}=18.1$  pN. Similar to the first experiment, the pretilt angle was found to be  $3.5^\circ$  through fitting. Because of this smaller pretilt angle, the maximum transmittance occurs at  $3.63 V_{\text{rms}}$  where  $\delta_0=\pi$ . By the same method as the first experiment,  $\tau_0$  was measured to be  $64 \pm 4$  ms. Theoretical calculation based on Eq.(5.5) gives  $\tau_0 \sim 52$  ms and the discrepancy is  $\sim 23\%$ . When the  $3.5^\circ$  pretilt angle is taken into consideration,  $\tau_0$  is calculated to be 56 ms from Eq.(5.13), which is closer to the

experimental result. Several other VA cells with various negative LC materials were also tested, and their pretilt angles are usually small ( $<2^\circ$ ). Under this circumstance, the effect of pretilt angle on the LC response time is insignificant. This result is also consistent with our theoretical analysis.

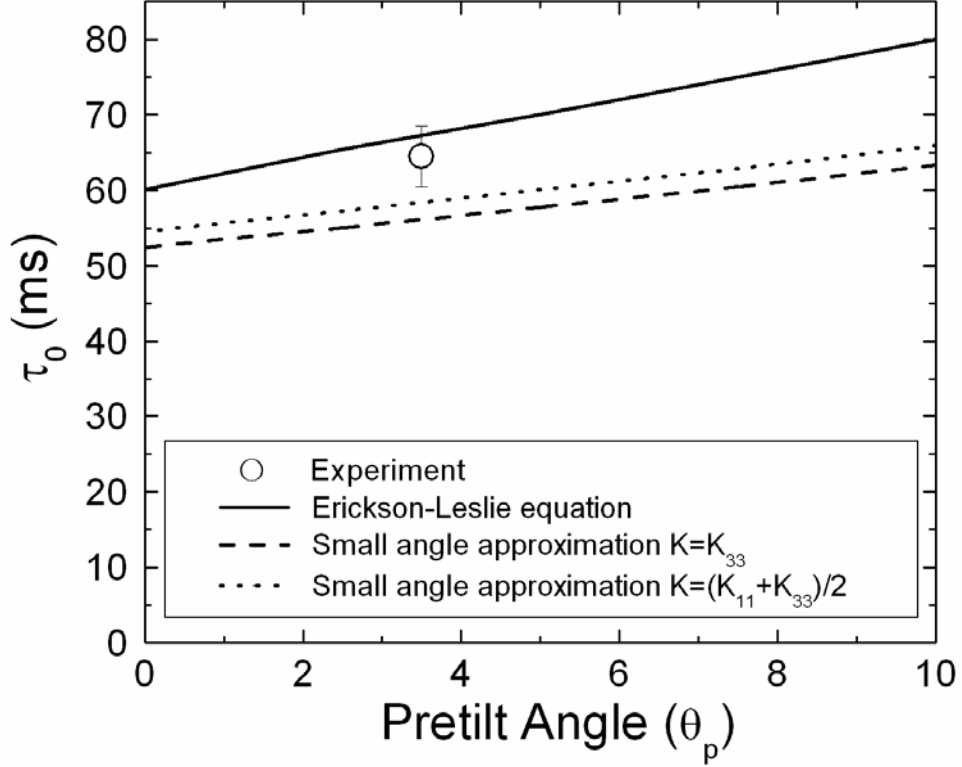


Figure 5.4: Pretilt angle  $\theta_p$  dependent LC response time  $\tau_0$ . Solid line represents the numerical solution of Erickson-Leslie equation [Eq.(5.1)]. The circle is the experimental result using LC mixture B. Dashed lines are the calculated results using Eq.(5.13), ( $K=K_{33}$ ), which employs the small angle and one-elastic constant approximations. Dotted lines are also calculated from Eq.(5.13), except that  $K_{33}$  is replaced by  $K=(K_{11}+K_{33})/2$ . Cell gap  $d = 7.10 \mu\text{m}$ , and bias voltage  $V_b = 3.63 V_{\text{rms}}$ .

FEM Numerical simulation based is employed to solve Eq.(5.1), which avoids the “one-constant approximation” and “small-angle approximation” used in the theoretical analyses. In Figure 5.4, the simulation results confirm that  $\tau_0$  increases as pretilt angle  $\theta_p$  gets larger, which is consistent with our theoretical analysis. Based on Eq.(5.13), two curves employing different elastic constant values,  $K=K_{33}$  and  $K=(K_{11}+K_{33})/2$ , are also plotted. To deal with dynamics of VA cells,  $K=K_{33}$  is usually used, but here the analytical results employing  $K=(K_{11}+K_{33})/2$  is closer to the simulated curve. In Eq.(5.1),  $K \sim K_{33}$  is accurate only when  $\theta$  is small. In a high voltage state, the LC directors tilt angle becomes relatively large so that the  $K_{11}$  term is pronounced. Thus, it seems more reasonable to take  $K_{11}$  into account and assume  $K \sim (K_{11}+K_{33})/2$ .

The discrepancy between the simulation and analytical results are mainly because of the single elastic constant ( $K_{33}=K_{11}$ ) and small angle approximations. In the small pretilt angle region ( $\theta_p \leq 2^\circ$ ), the difference is less than 11%. As  $\theta_p$  increases, the discrepancy slightly increases. The result in our second experiment is represented by the circle in Figure 5.4, and it agrees with the simulation and theoretical results reasonably well.

## CHAPTER SIX: CONCLUSION

This dissertation discusses the liquid crystal surface effects to meet challenges in liquid crystal applications for display and photonic systems. The novel techniques and theories discussed in this dissertation will be important for LC material development, LC alignment technique improvement and LC device designs.

One major work is that a high-electric-field approach is developed to characterize the anchoring energy of VA LC cells. VA LCDs has been widely used in LCD-TV applications, and it is important to measure the anchoring energy since it influences the LC electro-optic and dynamic performance significantly. The developed anchoring energy measurement method is also very helpful to improve LC alignment techniques. The wide-spread application of our practical measurement method in LCD industry is foreseeable.

Using the effective cell gap concept, we developed a new theory to quantitatively correlate anchoring energy to LC response time. Another approach is to employ the surface dynamic equation as the boundary conditions. The results of these two approaches are consistent. More importantly, we found that the conventional understanding of  $\tau \sim d^2$  is not valid under finite anchoring energy conditions. Instead,  $\tau$  is approximately proportional to  $d^x$ . Under two extreme (strong and weak) anchoring limits, the exponent  $x$  approaches 2 and 1, respectively. This finding is critical for optimizing liquid crystal devices, especially for LC cells with thin cell gap.

Pretilt angle effect on liquid crystal dynamics is also studied in the dissertation. Analytical expressions are derived to describe liquid crystal response time under nonzero pretilt angle conditions. The theoretical analysis is confirmed experimentally using vertically-aligned liquid crystal cells. This finding quantitatively correlates pretilt angles with liquid crystal response time, and is important for optimizing liquid crystal response time.

## LIST OF REFERENCES

- [1] I. C. Khoo and S. T. Wu, *Optics and Nonlinear Optics of Liquid Crystals* (World Scientific, Singapore, 1993).
- [2] M. Wand, W. N. Thurmes, R. T. Vohra, and K. M. More, "Advances in ferroelectric liquid crystals for microdisplay applications," *SID Digest* **27**, 157-161 (1996).
- [3] T. Ogawa, S. Fujita, K. Lwai, H. Koseki, "The trends of reflective LCDs for future electronic paper," *SID Digest* **29**, 217-220 (1998).
- [4] S. T. Wu and D. K. Yang, *Reflective Liquid Crystal Displays* (Wiley, New York, 2001).
- [5] M. F. Vuks, "Determination of the optical anisotropy of molecules of aromatic compounds from the double refraction of crystals," *Opt. Spectrosk* **20**, 644-651 (1966).
- [6] S. T. Wu, "Birefringence dispersions of liquid crystals," *Phys. Rev. A* **33**, 1270-1274 (1986).
- [7] F. Guerin, J. M. Chappe, P. Joffre, and D. Dolfi, "Modeling, synthesis and characterization of a millimeter-wave multilayer microstrip liquid crystal phase shifter," *Jpn. J. Appl. Phys.* **36**, 4409-4413 (1997).
- [8] Onsager, *L. Ann. NY Acad. Sci.* **51**, 627 (1949).

- [9] W. Maier and G. Meier, "A simple theory of the dielectric characteristics of homogeneous oriented crystalline-liquid phases of the nematic type," *Z. Naturforsch. Teil A* **16**, 262 (1961).
- [10] I. C. Khoo and S. T. Wu, *Optics and Nonlinear Optics of Liquid Crystals* (World Scientific, Singapore, 1993).
- [11] N. Ito, K. Sakamoto, R. Arafune, S. Ushioda, "Relation between the molecular orientations of a very thin liquid crystal layer and an underlying rubbed polyimide film," *J. Appl. Phys.* **88**, 3235 (2000).
- [12] M. Schadt, K. Schmitt, V. Kozenkov, V. Chigrinov, "Surface-Induced Parallel Alignment of Liquid Crystals by Linearly Polymerized Photopolymers," *Jpn. J. Appl. Phys. Part 1* **31**, 2155 (1992).
- [13] M. O'Neill, S. M. Kelly, "Photoinduced surface alignment for liquid crystal displays," *J. Phys. D: Appl. Phys.* **33**, R67 (2000).
- [14] Lee, K.-W.; Lien, A.; Stathis, J. H.; Paek, S.-H., "Control and Modification of Nematic Liquid Crystal Pretilt Angles on Polyimides," *Jpn. J. Appl. Phys.* **36**, 3591 (1997).
- [15] Sinha, G. P.; Wen, B.; Rosenblatt, C., "Large, continuously controllable nematic pretilt from vertical orientation," *Appl. Phys. Lett.* **79**, 2543 (2001).
- [16] H. Hatoh, K. Shohara, Y. Kinoshita, and N. Ookoshi, "Molecular tilt direction in a slightly tilted homeotropic aligned liquid crystal cell," *Appl. Phys. Lett.* **63**, 3577 (1993).

- [17] S. H. Paek, C. J. Durning, K.-W. Lee, A. Lien, “A mechanistic picture of the effects of rubbing on polyimide surfaces and liquid crystal pretilt angles,” *J. Appl. Phys.* **83**, 1270 (1998).
- [18] D. S. Seo, K. Muroi, and S. Kobayashi, “Generation of pretilt angles in nematic liquid crystal, 5CB, media aligned polyimide films,” *Mol. Cryst. Liq. Cryst.* **213**, 223 (1992).
- [19] J. Nehring, A. R. Kmetz, and T. J. Scheffer, “Analysis of weak-boundary-coupling effects in liquid-crystal displays,” *J. Appl. Phys.* **47**, 850-857 (1976).
- [20] X. Nie, R. Lu, H. Xianyu, T. X. Wu, S.T. Wu, “Anchoring energy and cell gap effects on liquid crystal response time”, *J. Appl. Phys.* **101**, 103110 (May 15, 2007).
- [21] E. Jakeman and E. P. Raynes, “Electro-optic response times in liquid crystals,” *Phys. Lett.*, **39A**, 69-70, Apr. 1972.
- [22] A. Rapini and M. Papoular, *J. Phys. (Paris), Colloq.* **30**, C-4 (1969).
- [23] A. Sugimura, G. R. Luckhurst and O. Y. Zhongcan, “Director deformation of a twisted chiral nematic liquid-crystal cell with weak anchoring boundaries,” *Phys. Rev. E* **52**, 681–689 (1995).
- [24] A. Lien, “A detailed derivation of extended Jones matrix representation for twisted nematic liquid crystal displays,” *Liq. Cryst.* **22**, 171-175 (1997).
- [25] J. E. Akin, *Finite Elements for Analysis and Design* (Academic Press, San Diego, 1994).
- [26] A. Taflove, S. C. Hagness, *Computational Electrodynamics: the Finite-Difference Time-Domin Method* (Artech House, Boston, 2000).

- [27] G. Panasyuk and D. W. Allender, "Approximate description of the three dimensional director and electric field in a liquid crystal display at a high voltage," *J. Appl. Phys.* **87**, 649-657 (2000).
- [28] R. C. Jones, "A new calculus for the treatment of optical systems. IV," *J. Opt. Soc. Am.* **32**, 486-493 (1942).
- [29] D. W. Berreman, "Optics in stratified and anisotropic media: 4×4 matrix formulation," *J. Opt. Soc. Am.* **62**, 502-510 (1972).
- [30] D. W. Berreman, "Optics in smoothly varying anisotropic planar structure: application to liquid crystal twist cells," *J. Opt. Soc. Am.* **63**, 1374-1380 (1973).
- [31] H. Wohler, G. Hass, M. Fritsch, and D. A. Mlynski, "Faster 4×4 matrix method for uniaxial inhomogeneous media," *J. Opt. Soc. Am.* **5**, 1554-1557 (1988).
- [32] P. Yeh, "Extended Jones matrix method," *J. Opt. Soc. Am.* **72**, 507-513 (1982).
- [33] C. Gu and P. Yeh, "Extended Jones matrix method II," *J. Opt. Soc. Am. A* **10**, 966-973 (1993).
- [34] A. Lien, "Extended Jones matrix representation for the twisted nematic liquid-crystal display at oblique incidence," *Appl. Phys. Lett.* **57**, 2767-2769 (1990).
- [35] F. H. Yu and H. S. Kwok, "Comparison of extended Jones matrices for twisted nematic liquid-crystal displays at oblique angles of incidence," *J. Opt. Soc. Am. A* **16**, 2772-2780 (1999).

- [36] Y. Huang, T. X. Wu, and S. T. Wu, "Simulations of liquid-crystal Fabry–Perot etalons by an improved 4×4 matrix method," *J. Appl. Phys.* **93**, 2490-2495 (2003).
- [37] X. Nie, T. X. Wu, Y. Lu, Y. H. Wu, X. Liang, and S. T. Wu, "Dual-frequency addressed infrared phase modulator with sub-millisecond response", *Mol. Cryst. Liq. Cryst.* **454**, 123-133 (2006).
- [38] S. T. Wu, "Phase retardation dependent optical response time of parallel-aligned liquid crystals," *J. Appl. Phys.* **60**, pp.1836 (1986).
- [39] S. T. Wu and C. S. Wu, "Experimental confirmation of the Osipov-Terentjev theory on the viscosity of nematic liquid crystals," *Phys. Rev. A*, **42**, pp.2219-2227, Aug. 1990.
- [40] G. Barbero, N. V. Madhusudana, and G. Durand, *J. Phys. (France) Lett.* **45**, L-613 (1984).
- [41] T. Marusiy, Yu. Reznikov, and V. Reshetnyak, *Sov. Phys. JETP* **64**, 502 (1986).
- [42] H. Yokoyama and H. A. van Sprang, "A novel method for determining the anchoring energy function at a nematic liquid crystal-wall interface from director distortions at high fields," *J. Appl. Phys.* **57**, 4520 (1985).
- [43] Yu. A. Nastishin, R. D. Polak, S. V. Shiyanovskii, and O. D. Lavrentovich, "Determination of nematic polar anchoring from retardation versus voltage measurements," *Appl. Phys. Lett.* **75**, 202 (1999).

- [44] K. H. Yang and C. Rosenblatt, "Determination of the anisotropic potential at the nematic liquid crystal-to-wall interface," *Appl. Phys. Lett.* **43**, 62 (1983).
- [45] Yu. A. Nastishin, R. D. Polak, S. V. Shiyankovskii, V. H. Bodnar, and O. D. Lavrentovich, "Nematic polar anchoring strength measured by electric field techniques," *J. Appl. Phys.* **86**, 4199 (1999).
- [46] F. Yang, L. Ruan, and J. R. Sambles, "Homeotropic polar anchoring energy of a nematic liquid crystal using the fully leaky waveguide technique," *J. Appl. Phys.* **88**, 6175 (2000).
- [47] A.I. Derzhanski, A.G. Petrov, and M.D. Mitov, *J. Phys. (Paris)* **39**, 273 (1978).
- [48] K. R. Welford and J. R. Sambles, "Analysis of electric field induced deformation in a nematic liquid crystal for any applied field," *Mol. Cryst. Liq. Cryst.* **147**, 25 (1987).
- [49] G. Carbone and C. Rosenblatt, "Polar anchoring strength of a tilted nematic: Confirmation of the dual easy axis model," *Phys. Rev. Lett.* **94**, 057802 (2005).
- [50] C. Rosenblatt, "Temperature-dependence of the anchoring strength coefficient at a nematic liquid crystal-wall," *J. Phys. (Paris)* **45**, 1087 (1984).
- [51] L. M. Blinov and V. G. Chigrinov, *Electrooptic Effects in Liquid Crystal Materials*, (Springer, New York, 1994).
- [52] S. T. Wu and D. K. Yang, *Reflective Liquid Crystal Displays*, (Wiley, New York, 2001).

- [53] X. Nie, Y. H. Lin, T. X. Wu, H. Wang, Z. Ge, and S. T. Wu, "Polar anchoring energy measurement of vertically aligned liquid-crystal cells," *J. Appl. Phys.*, **98**, pp. 013516, July 2005.
- [54] J. L. Erickson, "Conservation Laws for Liquid Crystals," *Trans. Soc. Rheol.*, **5**, pp. 23-34, Mar. 1961.
- [55] F. M. Leslie, "Some constitutive equations for liquid crystals," *Arch. Ration. Mech. Anal.*, **28**, pp. 265-283, 1968.
- [56] P. G. de Gennes and J. Prost, *The Physics of Liquid Crystals* (Clarendon Press, Oxford, 1993).
- [57] A. R. Kmetz, and F. K. von Willisen, *Nonemissive Electrooptic Displays*, (Plenum Press, New York, 1976).
- [58] A. A. Sonin, *"The Surface Physics of Liquid Crystals"* (Gordon and Breach, New York, 1995).
- [59] S. T. Wu and C. S. Wu, *J. Appl. Phys.* **65**, 527 (1989).
- [60] D. Armitage, I. Underwood, and S. T. Wu, *"Introduction to Microdisplays"* (Wiley, New York, 2006).
- [61] J. O. Kwag, K. C. Shin, J. S. Kim, S. G. Kim, and S. S. Kim, *SID Tech. Digest* **31**, 256 (2000).

- [62] A. Takeda, S. Kataoka, T. Sasaki, H. Chida, K. Ohmuro, and Y. Koike, *SID Tech. Digest* **29**, 1077 (1998).
- [63] Q. Wang and S. Kumar, "Submillisecond switching of nematic liquid crystal in cells fabricated by anisotropic phase-separation of liquid crystal and polymer mixture." *Appl. Phys. Lett.*, **86**, 071119, Feb. 2005.
- [64] T.J. Scheffer and J. Nehring, "Accurate determination of liquid-crystal tilt bias angles." *J Appl. Phys.*, **48**, pp. 1783-1792, May 1977.
- [65] H. Wang, T. X. Wu, X. Zhu, and S. T. Wu, "Correlations between liquid crystal director reorientation and optical response time of a homeotropic cell," *J. Appl. Phys.*, **95**, pp. 5502-5508, May 2004.
- [66] X. Nie, H. Xianyu, R. Lu, T. X. Wu, S.T. Wu, "Pretilt angle effect on liquid crystal response time", *IEEE/OSA Journal of Display Technology* (to be published).
- [67] X. Zhu, Z. Ge, T. X. Wu, and S. T. Wu, "Transflective liquid crystal displays," *J. Display Technology*, **1**, pp. 15-29, Sep. 2005.
- [68] D.K. Yang and S. T. Wu, *Fundamentals of Liquid Crystal Devices*, New York, Wiley, 2006.
- [69] M. F. Schiekkel and K. Fahrenschon, "Deformation of nematic liquid crystals with vertical orientation in electric fields," *Appl. Phys. Lett.* **19**, pp. 391-393, Nov. 1971.

- [70] K. H. Fan-Chiang, S. T. Wu, and S. H. Chen, "Fringing field effects on high-resolution liquid crystal microdisplays," *J. Display Technology*, **1**, pp. 304-313, Dec. 2005.
- [71] S. T. Wu and C. S. Wu, "High-speed liquid-crystal modulators using transient nematic effect," *J. Appl. Phys.*, **65**, pp. 527-532, Jan. 1989.
- [72] J. M. Geary, J. W. Goodby, A. R. Kmetz, and J. S. Patel, "The mechanism of polymer alignment of liquid-crystal materials," *J. Appl. Phys.*, **62**, pp. 4100-4108, Nov. 1987.
- [73] D. S. Seo, S. Kobayashi, and M. Nishikawa, "Study of the pretilt angle for 5CB on rubbed polyimide films containing trifluoromethyl moiety and analysis of the surface atomic concentration of F/C(%) with an electron spectroscope for chemical analysis," *Appl. Phys. Lett.*, **61**, pp. 2392-2394, Nov. 1991.
- [74] S. T. Wu and C. S. Wu, "Experimental confirmation of the Osipov-Terentjev theory on the viscosity of nematic liquid crystals," *Phys. Rev. A*, **42**, pp. 2219-2227, Aug. 1990.